Andrés Felipe Cortés Borray, Alejandro Garcés, Julia Merino, Esther Torres, Javier Mazón,

New energy bound-based model for optimal charging of electric vehicles with solar photovoltaic considering low-voltage network's constraints,

International Journal of Electrical Power & Energy Systems,

Volume 129,

2021,

106862,

ISSN 0142-0615,

https://doi.org/10.1016/j.ijepes.2021.106862

# New Energy Bound-Based Model for Optimal Charging of Electric Vehicles with Solar Photovoltaic Considering Low-Voltage Network's Constraints

Andrés Felipe Cortés Borray[a,b,*], Alejandro Garcés[c], Julia Merino[a,b], Esther Torres[b], Javier Mazón[b]
a TECNALIA, Basque Research and Technology Alliance (BRTA), Derio, Spain
b Department of Electrical Engineering, University of the Basque Country (UPV/EHU), Bilbao, Spain
c Department of Electric Power Engineering, Universidad Tecnológica de Pereira, Pereira, Colombia

*Corresponding author. Smart Grids and Energy Storage Area, TECNALIA, Astondo Bidea, Building 700, E-48160, Derio, Spain
E-mail address: acortes024@ikasle.ehu.eus

## Abstract

This paper introduces a linear programming (LP)-based optimisation method of charging electric vehicles (EVs) in a decentralised fashion. It exploits the available photovoltaic (PV) power to charge EV batteries while maintaining the low-voltage (LV) network within its operational limits. A new energy-bound model is implemented in order to meet the connected EVs energy requirements. This model highlights two main aspects: first, the proposed formulation seeks to compute both the upper and lower energy boundaries from the arrival energy and no from zero. Second, the charging power is dynamically adjusted by combining a fixed and variable charging rate to assure the technical limits of the network. This means maximising power delivered to all EVs for a given period by optimising the charging rate of each EV connected. Besides, a network sensitivity analysis technique is developed to manage voltage and loading constraints. The accuracy of the proposed linear approximation was tested simulating two cases (moderate and high penetration level of PVs and EVs) on a real LV feeder. Results over a set of simulations for winter and summer seasons demonstrate that this method can be effectively implemented as a charging strategy and for energy planning studies.

Keywords—Aggregator; Electric vehicle; Linear Programming; Load flow analysis; PV system; Unbalanced low voltage network

## 1. Introduction

Modern low voltage networks face a high presence of electric vehicles and renewable energy, motivated by the increasing concern about air quality and oil dependency. This trend is expected to continue in the coming years. Despite their clear advantages from the environmental point of view, these technologies present new challenges for their massive integration in the grid that require to be addressed with new operation methods. In particular, the charging of EVs needs to be optimised.

Drawbacks of the uncontrolled EVs charging process in LV networks have been widely studied by several researchers in [1–4]. All these studies conclude that this passive strategy causes significant voltage drops and overloads on the LV feeders. Moreover, with an increasing level of PV penetration in the distribution networks, reverse power flow and voltage rise would also be expected [5]. Therefore, these effects can lead to an expensive investment and time-consuming tasks to reinforce network capacity. In order to deal with these problems, there would be a need to stimulate the self-consumption of PV power for charging the EV battery when possible. This means taking advantage of the correlation between both distributed energy resources, which mainly depends on the driver's mobility uses, the PV

power forecast and the implementation of an effective smart control strategy. For instance, a user with several daily trips near to its household benefits from almost 70% of PV power generation during the charging process, whereas a user with a long-range trip would take less advantage of that power availability [6]. Thereby, this highlights the potential to further redistribute the EV charging process to better match with PV power generation. Besides, this aspect is also influenced by the weather conditions, *i.e.*, the EV owners will tend to charge their batteries early on a sunny day, reducing the electric power demand at peak hours. However, it would be required devise new controlled charging schemes in a centralised, distributed or decentralised mode, as classified in [7]. Since centralised methods require full network visibility and handling a significant amount of information to be transmitted and processed, the decentralised and distributed schemes are more attractive because they can be gradually implemented and use local communications [2,8].

Hence, in [1,9–12], different researchers have studied the use of network sensitivity coefficients to approximate the voltage, loading level or both in unbalanced LV networks when adding new loads such as EVs. These studies have used such coefficients within different optimisation techniques (e.g., linear [1,9,11], nonlinear [10] and heuristic [12]) to coordinate in a centralised manner the charging process of EVs. Nonetheless, these studies do not consider the addition of photovoltaic systems to assess in conjunction with the EVs their impact on the LV network. In [13], the authors employed mixed-integer linear programming (MILP) to minimise the energy storage systems (ESS) charging power in EV stations for providing voltage support in unbalanced feeders with PVs. This study only considered the voltage level as the network constraint, which was assessed just using a set of sensitivity coefficients that combine load and generation. In [9], the load level increase for both the network's transformer and lines due to power demanded by the EVs is evaluated based on their sensitivity coefficients expressed in *kVA/kW*. This criterion is also used in [11] for assessing the loading level on the distribution transformer. Likewise, in [1], the load variation on the main cable is evaluated by these sensitivities expressed in *A/kW*. However, apparent power and current are complex values whose magnitudes are always positive. Therefore, the way of expressing these sensitivities is valid only if load addition is considered (*i.e.*, the EVs). Nonetheless, this is no longer valid if the power flow changes its direction because of excess intermittent renewable electricity. This means that the reverse power flow in the network cannot be computed through those magnitudes within the linearization. Hence, by considering PV generation, the loading sensitivity coefficients for lines and distribution transformers must be calculated in terms of the active power (*kW/kW*) to evidence the power flow direction.

On the other hand, [14] proposed an aggregate power- and energy-boundary model for EVs with vehicle-to-grid (*V2G*) capacity to provide power reserve services to the grid. The model is included as a constraint in a day-ahead scheduling problem formulated as a mixed-integer nonlinear programming (MINLP) model. In [15], a similar energy-bound model for *V2G*, along with a charging power allocation algorithm to offer power reserve services are introduced. Here, the upper and lower energy boundaries of EVs are computed in real-time as a function of the battery voltage, current, charging/discharging rate, and the state-of-charge (*SOC*). As this model requires extensive information about the EV, for a large number of EVs, it will be computationally more intense.

Additionally, other energy models are used only for charging EVs as part of different charging strategies based on quadratic programming (QP) [16] and LP [16–18] techniques. For example, in [16], the upper

and lower energy limits are obtained by considering the electrical power demand during driving with the maximum and minimum energy capacity of the battery, respectively. These last two constants are also used in [14]. Moreover, both authors use of a nonlinear battery model to compute the initial energy of EVs using an extensive set of parameters. The work described in [17] and [18] use similar equations to compute the energy boundaries of the EVs. Both define the arrival energy state as zero, which then increases up to the required energy level of each EV. Besides, these studies, excluding [16], do not consider any network topology or related technical constraints.

Unlike the literature mentioned above, the proposed energy boundary model here highlights two main aspects: first, the proposed formulation seeks to compute both the upper and lower energy boundaries from the arrival energy and no from zero (based on the required energy level). Second, the charging power is dynamically adjusted by combining a fixed and variable charging rate to assure the technical limits of the network. Furthermore, this paper proposes a linearization of network constraints throughout a series of sensitivity coefficients by accounting for the simultaneous effect of PV power and EV charging on the LV networks. Hence, this paper focuses on proposing a decentralised charging control strategy, as classified in [7], based on the energy and power boundaries of EVs and the use of the available PV power generation. A new formulation of the energy-bound model is introduced considering the uncertainty behaviour of EVs. This decentralised control is envisaged for a small network zone where an aggregator or a distribution system operator (DSO) can manage and monitor, through a small central controller, all the available resources, *i.e.*, EVs and PVs. The proposed methodology is formulated as a linear programming model due to its capability to find optimal global solutions in an efficient way. Unbalanced three-phase load flows are used to generate the network sensitivity coefficients, which are subsequently used in the definition of network constraints (*i.e.*, voltages and loading level). The final objective is to find in a decentralised fashion the best charging pattern that meets the energy requirements of every EV connected to the LV network, taking advantage of the PV power while maintaining the network within its operational limits.

This article is organised as follows: Section 2 explains the uncertainty behaviour for EVs and PVs, the proposed energy-boundary model and PV system model approximation. Section 3 describes the network sensitivities and the proposed objective function with its constraints. In Section 4, the case studies are introduced, and Section 5 discusses the numerical results. Finally, conclusions are presented in Section 6.

## 2. Distributed Energy Resources Modelling

### 2.1. Uncertainty characterisation of EVs

It is assumed that the arrival and commuting processes of the EVs are all uncertain. However, these variables follow known probability distributions and their parameters can be predicted based on historical records. In this regard, the daily travelled distance $d_j$ is evaluated from real data [19] by a lognormal distribution function with parameters $\mu_{tra}$ and $\sigma_{tra}$. Likewise, the truncated normal distribution $\varphi$ is adopted from [20] to represent the arrival time $t_j^{arr}$ of each EV as follows:

$$t_j^{arr} = \varphi(N_{EV} \mid \mu_{arr}, \sigma_{arr}, t_{\min}, t_{\max}) \tag{1}$$

where $N_{EV}$ is the number of EVs parked at home, $t_{\min}$ and $t_{\max}$ denote the arrival time range of EVs with mean $\mu_{arr}$ and standard deviation $\sigma_{arr}$. Parameters and detailed formulation for both probability density functions are shown below in Table 1 and Appendix A, respectively.

Table 1
Parameters of the probability density functions

| Variable | Input | PDF | Parameters | | | |
|---|---|---|---|---|---|---|
| $d_j$ | $N_{EV}$ | Lognormal | $\mu_{tra}$ = 2.89257 | $\sigma_{tra}$= 0.91779 | | |
| $t^{arr}$ | $N_{EV}$ | Truncated Normal | $\mu_{arr}$ = 16:00 | $\sigma_{arr}$= 3-h | $t_{min}$ = 11:00 | $t_{max}$ = 23:00 |

## 2.2 EVs model

The batteries of the EVs are evaluated as a black box. This means that the charging efficiency of the batteries does not depend on the charge power $P_j^{ch}$, which can take any positive value within a certain range of nominal battery performance. This approach simplifies the model in comparison with the nonlinear representation used in [4].

In order to quantify the desired energy level of an EV's battery $e_j^{obj}$ when connected, first, it is necessary to compute another set of energy levels. Thus, the arrival energy level $e_j^{arr}$ of the *jth* EV is determined based on its maximum battery capacity $e_j^{B\max}$, which is derived from the maximum state-of-charge $SOC_{\max}$ and rated battery capacity $BC_j$ in *kWh* from Eq. (2), as well as the energy consumption rate $ECR_j$ and the daily travelled distance $d_j$ in *km*, as given in Eq. (3). The *ECR* is defined as the estimated average ratio of the electrical energy used per kilometre travelled for In-city, Highway, or Combined driving modes, expressed in *kWh/km*.

$$e_j^{B\max} = SOC_{\max} \cdot BC_j \tag{2}$$

$$e_j^{arr} = e_j^{B\max} - ECR_j \cdot d_j \tag{3}$$

Based on the arrival energy level, the desired energy level of the battery $e_j^{obj}$ and the required energy level $e_j^{req}$ can be obtained as follows:

$$e_j^{obj} = SOC_{obj} \cdot BC_j \tag{4}$$

$$e_j^{req} = \frac{SOC_{obj} \cdot BC_j - e_j^{arr}}{\eta_{ch}} \tag{5}$$

where $\eta_{ch}$ is the charger efficiency, and the desired state-of-charge $SOC_{obj}$ can be set to a specific value lower than or equal to the $SOC_{\max}$; which is decided by the owner.

Additionally, the minimum energy level of the *jth* EV's battery $e_j^{B\min}$ in Eq. (6) is used to verify that initial levels of $e_j^{arr}$ and $e_j^{obj}$ are feasible to be assessed. This is calculated iteratively for each EV throughout an embedded For-While loop according to the flowchart in Fig. 1. Note that for a real application of the proposed method, both $t_j^{arr}$ and $e_j^{arr}$ can be directly obtained from the energy management system (EMS) of the EVs when it is connected. Therefore, it is not necessary to consider both Eq. (3) and the flowchart. However, for energy planning studies, the whole method should be followed, as stated in this paper.

$$e_j^{B\min} = SOC_{\min} \cdot BC_j \tag{6}$$

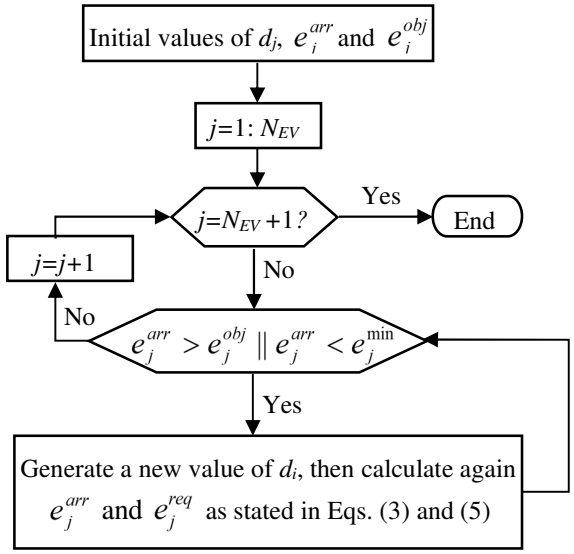


Fig. 1. Flowchart for verifying energy levels per EV based on the samples of driven distance

Having considered charger efficiency within the required energy level in Eq. (5), the expected parking time $t_j^p$ of the *jth* EV in Eq. (7) is obtained based on its maximum DC charging power $P_{ch}^{\max}$. Note that it may vary due to the type of connection (single- or three-phase) and charging standards [21].

$$t_j^p = ceil\left\{\frac{e_j^{req}}{P_{ch}^{\max}}\right\} \tag{7}$$

Therefore, the expected disconnection time $t_j^{dis}$ for vehicle *j* is determined the summation of the arrival time $t_j^{arr}$ and parking time $t_j^p$:

$$t_j^{dis} = t_j^{arr} + t_j^p \tag{8}$$

2.3. Energy boundaries of EVs

Under the control of an aggregator, an EV *j* with a scheduled parking time has flexible charging capacity through its energy and power boundaries, which define a possible set of charging paths [22]. Thereby, the upper energy boundary $e_j^{upper}$ obeys to an immediate charging process up to reach the desired energy level, which can be lower than or equal to the maximum battery capacity. In contrast, the lower energy boundary $e_j^{lower}$ represents the curve with the maximum time delay $\left(t_j^{delay}\right)$ of the charging process. Conversely, the power boundaries refer to the instantaneous rated charging power at each time slot while the EV remains connected. However, before computing the energy boundaries, it is required to evaluate the number of discrete-time intervals $t_j^{\text{int}}$ for each EV parked at home by considering a time step $t_s$ and an interval length $\Delta t = t_s/60$, as follows:

$$t_j^{\text{int}} = \frac{t_j^p}{\Delta t} \tag{9}$$

Based on $t_j^{arr}$ and $t_j^{\text{int}}$, the energy boundaries for vehicle *j* are determined using the proposed recursive discrete-time equations in (10) and (11). In this model, the upper energy limit is quantified starting from the arrival energy level of the *jth* EV up to the estimated plug-out time, *i.e.*, it goes from a present state up to a future one. Conversely, the lower energy boundary is computed from the objective energy level of the *jth* EV up to reach the arrival energy level, *i.e.*, it goes from a future condition up to a present one. Moreover, these expressions, in conjunction with the network's constraints, assure that during the optimisation process, the charging path of every EV remains within their energy limits.

$$e_{j,(t_j^{arr}+k)}^{upper} = \begin{cases} e_j^{arr}, & k = 0 \\ \min\left\{ e_{j,(t_j^{arr}+k-1)}^{upper} + P_{ch}^{\max} \cdot \eta_{ch} \cdot \Delta t,\, e_j^{obj} \right\}, & k = 1, \mathrm{K}\,, t_j^{\text{int}} + 1 \end{cases} \quad \forall j \in \Omega_{EV} \tag{10}$$

$$e_{j,(t_j^{arr}+t_j^{\text{int}}-k)}^{lower} = \begin{cases} e_j^{obj}, & k = 0 \\ \max\left\{ e_{j,(t_j^{arr}+t_j^{\text{int}}-k+1)}^{lower} - P_{ch}^{\max} \cdot \eta_{ch} \cdot \Delta t,\, e_j^{arr} \right\}, & k = 1, \mathrm{K}\,, t_j^{\text{int}} + 1 \end{cases} \quad \forall j \in \Omega_{EV} \tag{11}$$

In detail, Eq. (10) ensures that the upper energy state of the EV *j* is equal to the arrival energy at $t_j^{arr}$ and in later periods $\left(t_j^{arr} + k\right)$ could only be at most $P_{ch}^{\max} \cdot \eta_{ch} \cdot \Delta t$ greater than the energy remaining from the previous period $\left(t_j^{arr} + k - 1\right)$. Moreover, it should also be no larger than the objective energy level. Eq. (11) foresees that the lower energy state of each EV at time $t_j^{dis}$ must match with the objective energy level and in previous periods $\left(t_j^{arr} + t_j^{\text{int}} - k\right)$ could be at most $P_{ch}^{\max} \cdot \eta_{ch} \cdot \Delta t$ lower than its value at $\left(t_j^{arr} + t_j^{\text{int}} - k + 1\right)$ but cannot be lower than the arrival energy level. Fig. 2 exemplifies the energy boundaries of an EV *j*, which energy level follows an optimal charging trajectory up to reach the objective energy state insofar that set-point does not change if a) $e_j^{arr} \geq e_j^{B\,\min}$ or b) $e_j^{arr} = e_j^{B\,\min}$.

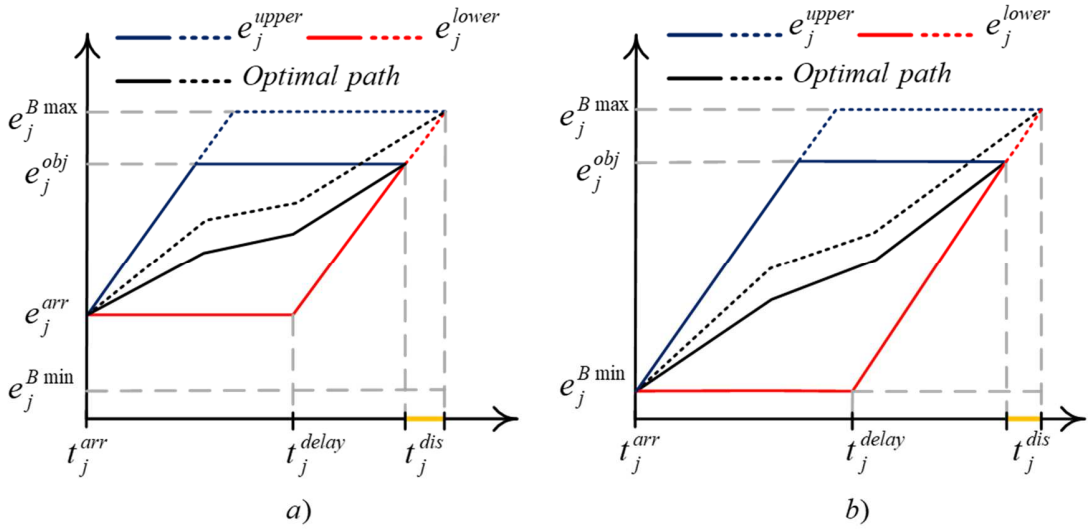


Fig. 2. Energy boundaries of a scheduled EV with a) $e_j^{arr} \geq e_j^{B\min}$ and b) $e_j^{arr} = e_j^{B\min}$

## 2.4. PV systems model

The yearly solar irradiance and ambient temperature data are collected from [23] for modelling the uncertainty of PV generation. These data are used to obtain the estimated daily power production of a single-phase PV system by using the method of Araujo-Green [24] as shown in the boxplot[1] of Fig. 3.

Based on the PV power forecast, a math approximation for modelling the output power of PV inverters is proposed for the summer and winter seasons as presented in Fig. 3. Power is represented as a shifted cosine wave squared to smooth its edges with the peak at noon, as given in Eq. (12). Note that this fitting function also describes the uncertainty of PV power by considering the standard deviation value $\sigma$ from the data used above.

$$P_{i,t}^{PV} = P_i \cdot \cos\left(a \cdot \frac{2\pi}{N_{slots}}\left(t - \frac{N_{slots}}{2} - b\right)\right)^2 \pm \sigma \quad \forall i \in \Omega_N \neq \emptyset, t = [0, N_{slots}] \tag{12}$$

where coefficients $a$, $b$ define the period and wave shifting, and parameters $c$, $d$, allow truncating to zero the signal from $t = 0$ to $N_{slots}/c$ and from $t = (N_{slots} - N_{slots}/c - d)$ to $N_{slots}$ in order to represent the absence of sunshine. Moreover, $P_i$ is a power set point of the inverter connected at the household $i$, $P_{i,t}^{PV}$ is the output power of the inverter hooked up at the household $i$ at time $t$, and $N_{slots}$ is the number of time slots for evaluating the model. For any evaluation period $T$, $N_{slots} = T/\Delta t$. All model parameters are given in Appendix B.

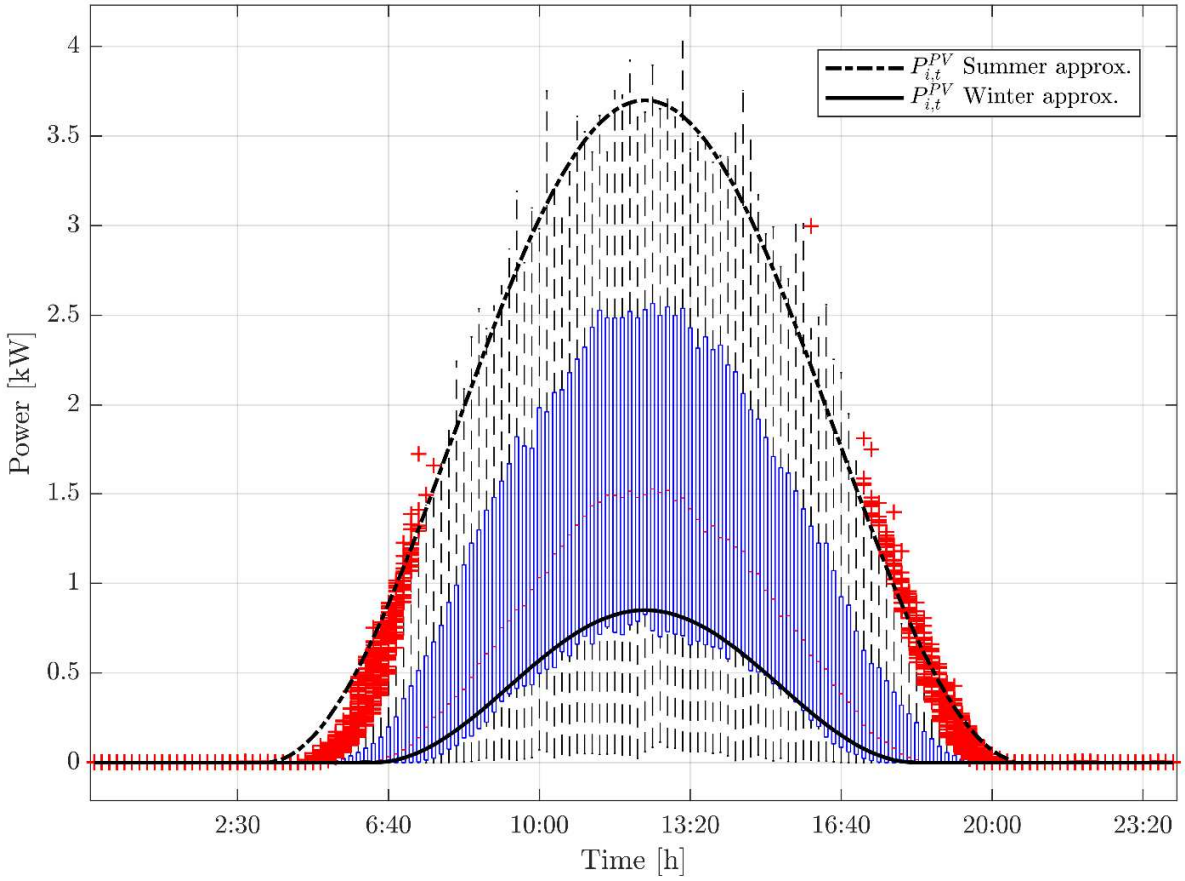


Fig. 3. Boxplot for the PV inverter power derived from yearly meteorological data by using the model of Araujo-Green. Fitted approximations of PV inverter power for summer (dashed line) and winter (continuous line) seasons.

1 Boxplot: The line that splits the box into two parts indicates the median of the data. The box represents the distance between the upper and lower quartiles, which is known as the interquartile range (IQR). The upper and lower lines are known as whiskers, which mark the data extremes. The whiskers also provide information about symmetry in the tails of the distribution. Any points lying outside the 1.5 × IQR around the box are known as "outliers" and are denoted by + symbols.

## 3. Optimisation method

### 3.1. Network sensitivities

Unbalanced three-phase load flows in steady-state are used to generate the network sensitivity coefficients, which are subsequently used in the definition of network constraints. This task is performed using PowerFactory (*PF*) [25] in conjunction with Python [26]. In order to get the sensitivity values due to the addition of load and generation, a steady load of 1 kW is initially assigned to each household, which is the maximum average demand from all used power profiles. Then a load flow is solved to record the loading levels per phase on lines and distribution transformers, as well as the voltage at each household. Subsequently, load increases up to 2 *kW* at the first household, then the load flow is executed again, and the new results from the specified points on the network are stored. This data is then used to compute the sensitivities of voltage and loading due to the addition of load. For example, the voltage

sensitivity is calculated as $\partial V/\partial P = \left(V_i^{new} - V_i^{base}\right)/\left(P_i^{new} - P_i^{base}\right)$, where $V_i^{base}$ and $V_i^{new}$ represent the initial and new voltage level from the load flow due to the change in the steady-state power at every load *i*. A similar approach is considered for computing the loading sensitivities. To reflect the addition of generation, the initial load changes to 0 *kW*. Voltage and loading sensitivities for the network components of interest are obtained in the same manner. Note that before varying a new household load, the previous one is restored to its original power level. This routine is repeated for the whole set of households, lines and distribution transformers to obtain the sensitivity coefficients of the network. Only one set of sensitivities is calculated along the test period, as this reduces the computational burden and execution time of the algorithm. However, these sensitivity values cannot be expected to match those in which the load continually varies on the feeder. But these sensitivities allow quantifying the impact that multiple EVs and PVs, charging and injecting power simultaneously, can have on a particular node, service cable and distribution transformer on the network.

3.2. Objective function

With the energy boundaries, the aggregator seeks to coordinate the charging of all EVs to maximise customer satisfaction taking advantage of the available PV power without violating grid technical limits. Thereby, during the daytime charging of EVs, the proposed optimisation aims to improve the self-consumption of PV power and reduce the dependence on the network. This means maximising power delivered to all EVs for a given period by optimising the charging rate of each EV connected. The optimised charging profile is centrally calculated based on an LP model which assures an even distribution of the power at each time slot for all EVs. Mathematically, the optimisation problem to be solved at *t* is as given:

$$\underset{\forall i \neq \emptyset}{Max}\ f = \sum_{i=1}^{H} \sum_{t=0}^{N_{slots}} \left(P_{i,t}^{EV} - \Delta_{i,t}^{P\,inc}\right) \cdot x_{i,t} \tag{13}$$

where *H* denotes the number of households being supplied by the DSO, and $x_{i,t}$ is a binary matrix $(x)_{H \times N_{slots}}$ such that $x_{i,t} = 1$ if the EV *j* is connected to the household *i* at time *t*, and 0 otherwise. It should be noted that $t_j^{\text{int}}$ settles the availability span for vehicle *j* when it is connected to the household *i*. Additionally, $P_{i,t}^{EV} = P_{i,t}^{ch} \cdot \eta_{ch}$ is the charging power in *kW* for the vehicle connected to the household *i* at time *t*, which can vary from zero up to the rated power of the charger. $\Delta_{i,t}^{P\,inc}$ is the increase in the rate of charge in *kW* for the vehicle connected to the household *i* at time *t*. This term is introduced as a penalty deviation variable to handle conditions in which a fixed rate of charge ($\Delta_P$) cannot be satisfied due to the lower energy boundary from constraint (17). Both $P_{i,t}^{EV}$ and $\Delta_{i,t}^{P\,inc}$ are continuous decision variables. In the set of households $\Omega_H$, $\emptyset$ means that the optimisation problem discards the houses without a PV, an EV or both. This reduces the number of variables and constraints, and therefore the computational burden. However, in the post-optimisation process, such households are evaluated based on the outcomes obtained from the method.

### 3.3. Constraints

The objective function from Eq. (13) is subject to a series of constraints at each time slot to ensure a proper network operation with the embedded PV generation while supplying households and EVs demand.

#### 3.3.1. EVs constraints

Based on the energy level of EV batteries, the charging rate of EVs is dynamically adjusted without violating grid technical limits as follows:

$$0 \le P_{i,t}^{EV} \le P_{ch}^{\max} \cdot \eta_{ch} \quad \forall i \ne \emptyset \in \Omega_H, \forall t \tag{14}$$

$$P_{i,(t-1)}^{EV} - \left(\Delta_P + \Delta_{i,t}^{P\,inc}\right) \le P_{i,t}^{EV} \le P_{i,(t-1)}^{EV} + \left(\Delta_P + \Delta_{i,t}^{P\,inc}\right) \quad \forall i \ne \emptyset \in \Omega_H, \forall t \tag{15}$$

$$0 \le \Delta_{i,t}^{P\,inc} \le \Delta_{\max}^{P} \quad \forall i \ne \emptyset \in \Omega_H, \forall t \tag{16}$$

$$e_{i,(t_j^{arr}+k)}^{lower} \le e_{i,(t_j^{arr}+k)}^{EV} \le e_{i,(t_j^{arr}+k)}^{upper} \quad k = 0, \mathrm{K}, t_j^{\mathrm{int}} + 1, \forall i \in \Omega_H \ne \emptyset, \forall j \in \Omega_{EV} \tag{17}$$

$$e_{i,(t_j^{arr}+k)}^{EV} = \begin{cases} e_i^{arr} + P_{i,(t_j^{arr}+k)}^{EV} \cdot \Delta t & , \; k = 0 \\ e_{i,(t_j^{arr}+k-1)}^{EV} + P_{i,(t_j^{arr}+k)}^{EV} \cdot \Delta t \,, & k = 1, \mathrm{K}, t_j^{\mathrm{int}} + 1 \end{cases} \quad \forall i \ne \emptyset \in \Omega_H, \forall j \in \Omega_{EV} \tag{18}$$

Following the linear objective function, Eq. (14) imposes that the charging power for the vehicle connected to the household *i* cannot exceed its power boundaries at any time step. Eq. (15) limits significant variations in the charging rate for consecutive time slots through a fixed set-point of $\Delta_P$ that can be relaxed only when necessary using the penalty deviation variable $\Delta_{i,t}^{P\,inc}$. This occurs for vehicles with narrow energy boundaries where a power boost is needed in the next time step for not violating the lower energy bound. Eq. (16) ensures that an increase in the charging rate of the EV connected to the household *i* should be no larger than the remaining capacity of the charger $\left(\Delta_{\max}^{P} = P_{ch}^{\max} \cdot \eta_{ch} - \Delta_P\right)$. Eq. (17) states that the energy level for vehicle *j*, which is connected to household *i*, at every time *k* is within its energy boundaries. This energy state is detailed in Eq. (18) for the arrival time interval of vehicle *j* $\left(t_j^{arr}\right)$ and later periods by considering the energy remaining from the previous period $\left(t_j^{arr} + k - 1\right)$ and the charging power at time *k*. Note that the indexes notation in Eq. (17) differs from Eqs. (10)–(11) by considering the household *i* to which the EV *j* is connected.

#### 3.3.2. Network constraints

The addition of EVs and PVs along the network may cause a significant drop or rise in voltage magnitude at every load node. This depends on several factors, which includes the charging rate of the EV, the power injected by the PV system and their location in the network. To ensure that voltage magnitude is within the operating limits defined by the DSO, the following constraint is defined:

$$V_{\min} \le V_{i,t}^{base} + \alpha_{i,i} \cdot P_{i,t}^{EV} + \beta_{i,i} \cdot P_{i,t}^{PV} + \sum_{h=1}^{H} \left( \alpha_{h,i} \cdot P_{h,t}^{EV} + \beta_{h,i} \cdot P_{h,t}^{PV} \right) \le V_{\max}, \quad (19)$$
$$\forall i, h \ne \emptyset \in \Omega_H, i \ne h, \forall t$$

where $V_{i,t}^{base}$ is the base voltage at the *ith* household node, $\alpha_{i,i}$ and $\beta_{i,i}$ represent the sensitivity of voltage $(\partial V / \partial P)$ at household node *i* due to power supplied to the EV *i* and power generated by the PV system *i*, $\alpha_{h,i}$ and $\beta_{h,i}$ are the sensitivity of the voltage for household *i* as a result of power demanded by the EV *h* and power produced by the PV system *h*. Note that a negative sensitivity value in $\alpha$ represents a voltage drop in such node, while in $\beta$ that value will be positive, which indicates a voltage rise. Additionally, $V_{\min}$ and $V_{\max}$ define the minimum and maximum permissible network voltage levels. It should also be noted that $\alpha$ and $\beta$ are two square matrices of $[H \times H]$, and the term $i \ne h$ means that *i* remains fixed while *h* varies.

In addition to voltage levels, further constraints for maintaining the active power flow within limits are evaluated. This means that it is necessary to consider how the active power variation of PVs and EVs affects the loading level of the entire network by making use of the sensitivity coefficients. The proposed linearization for power flowing through the cables and distribution transformers of the LV-network is presented as follows:

$$P_{Line\,i,\phi,t}^{base} + \sum_{k=1}^{H} \left( \mu_{k,\phi,i} \cdot P_{k,t}^{EV} + \lambda_{k,\phi,i} \cdot P_{k,t}^{PV} \right) \le P_{Line\,i,\phi}^{\max}, \quad (20)$$
$$\forall i \in \Omega_L, \forall k \ne \emptyset \in \Omega_H, \forall \phi, t$$

$$P_{Tx\,i,\phi,t}^{base} + \sum_{k=1}^{H} \left( \delta_{k,\phi,i} \cdot P_{k,t}^{EV} + \varepsilon_{k,\phi,i} \cdot P_{k,t}^{PV} \right) \le P_{Tx\,i,\phi}^{\max}, \quad (21)$$
$$\forall i \in \Omega_{Tx}, \forall k \ne \emptyset \in \Omega_H, \forall \phi, t$$

where $P_{Line\,i,\varphi,t}^{base}$ and $P_{Tx\,i,\varphi,t}^{base}$ are the base loading levels in *kW* for the supplying cable *i* and distribution transformer *i* per phase $\varphi$ at time *t*. Moreover, $\mu_{k,\varphi,i}$, $\delta_{k,\varphi,i}$ and $\lambda_{k,\varphi,i}$, $\varepsilon_{k,\varphi,i}$ are the loading sensitivity coefficients for each phase $\varphi$ of the service cable *i* and transformer *i* due to power demanded by vehicle *k*, and power generated by PV system *k*, both in *kW*. Note that a positive sensitivity value in $\mu$ and $\delta$ represents an increase of the loading level on the main cable, whereas, in $\lambda$ and $\varepsilon$, those values will be negative, which indicates a reduction in the loading level. All these coefficients are three-dimensional matrices of $[H \times \varphi \times (Line\ \&\ Tx)]$. Lastly, $P_{Line\,i}^{\max}$ and $P_{Tx\,i}^{\max}$ is the rated capacity in *kW* for both the service cable *i* and the distribution transformer *i*. Note that the initial voltage at households nodes and the base loading levels on main cable and distribution transformer are calculated beforehand as parameters through the unbalanced quasi-dynamic power flow for the test period *T* in PowerFactory.

To exemplify the interaction between the aggregator from zone *k* and the household *i*, Fig. 4 shows a detailed structure including the PV inverter, EV charger, demand profile of the customer, and the embedded control. The unit with the embedded controller can manage and communicate with the power inverter, charger, and battery management system of the EV. In this study, only the computed charging

power for the time interval $[t_j^{arr}, t_j^{dis}]$ is sent to each charging spot, once the optimisation problem has been solved. Therefore, at the end of the charging process, it is expected that each EV has reached its desired energy level based on Eq. (22). Lastly, Fig. 5 outlines the simplified procedure of the proposed centralised control method.

$$e_i^{end} = e_i^{arr} + \sum_{t=t_i^{arr}}^{t_i^{dis}} P_{i,t}^{EV} \cdot \Delta t \quad \forall i \neq \emptyset \in \Omega_H \tag{22}$$

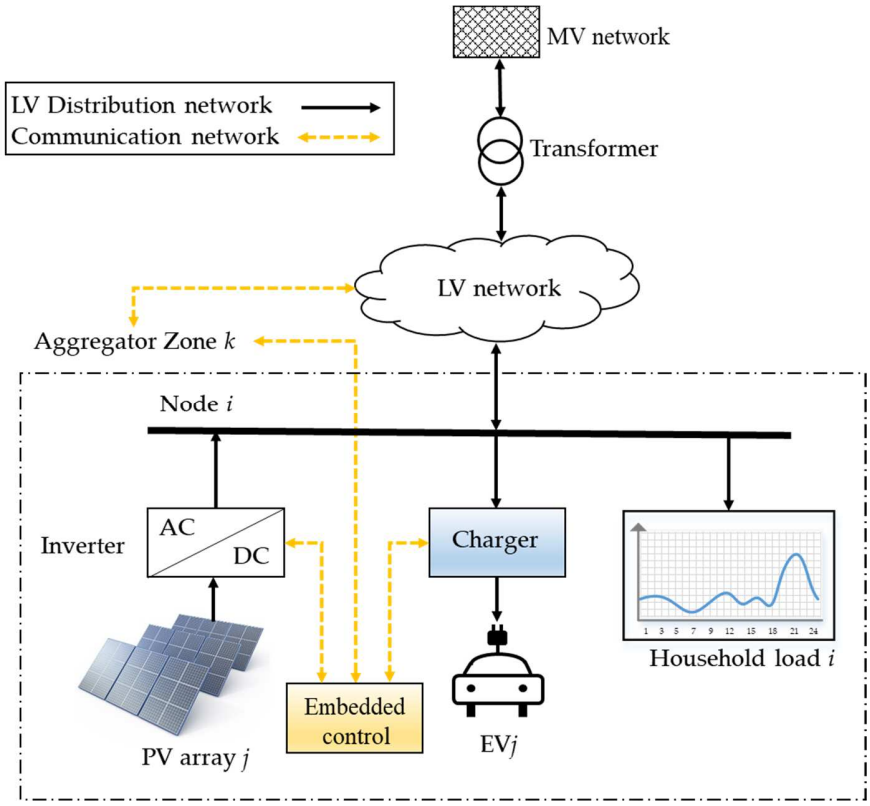


Fig. 4. Interaction between aggregator from zone *k* and household *i*

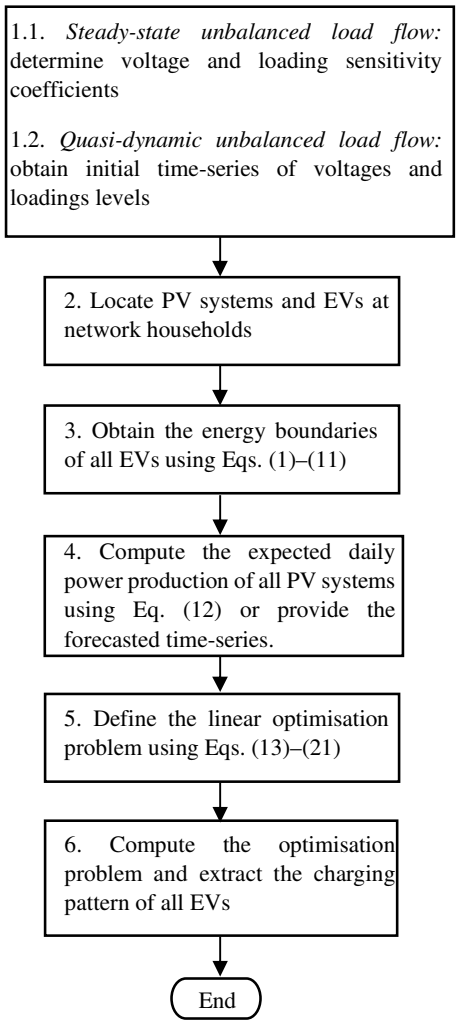


Fig. 5. Simplified flowchart of the proposed methodology

## 4. Case Studies

A feeder has been extracted from one real LV network in the North West of England [27] to investigate the applicability of the proposed method. This feeder is also known as the IEEE European Low Voltage Test Feeder. However, as this benchmark feeder does not physically consider the neutral conductor due to the Kron's reduction, the data was extracted from the original feeder. This radial distribution feeder supplies power to 55 single-phase households unevenly distributed per phase through 1.431 km of cables. This means that exist an unbalanced condition in the network with most of the loads connected to phase *A*. The feeder is connected to 11 *kV* medium-voltage network through an 800 *kVA* distribution transformer with a delta/grounded-wye connection. The rated phase-to-phase voltage at the secondary of the transformer is 400 *V* with $\pm 10\%$ allowable variation. It is assumed that the cross-section of the neutral conductor equals to phase conductor for both the three- and single-phase service cables. Specifications for

the network model components can be found in [28]. The one-line diagram of the feeder is shown in Fig. 6, which is fully modelled using *PF*.

The load curve for each household was obtained from a pool of 100 load profiles given in [27,28], which were assigned in ascending order to each home. These time-series reproduce real patterns of domestic power consumption with a resolution of one minute. However, in this study, load profiles are subsequently downsampled to a time-series with a 10-minute time step. The loads are modelled as constant power (*P*) at a lagging power factor of 0.95.

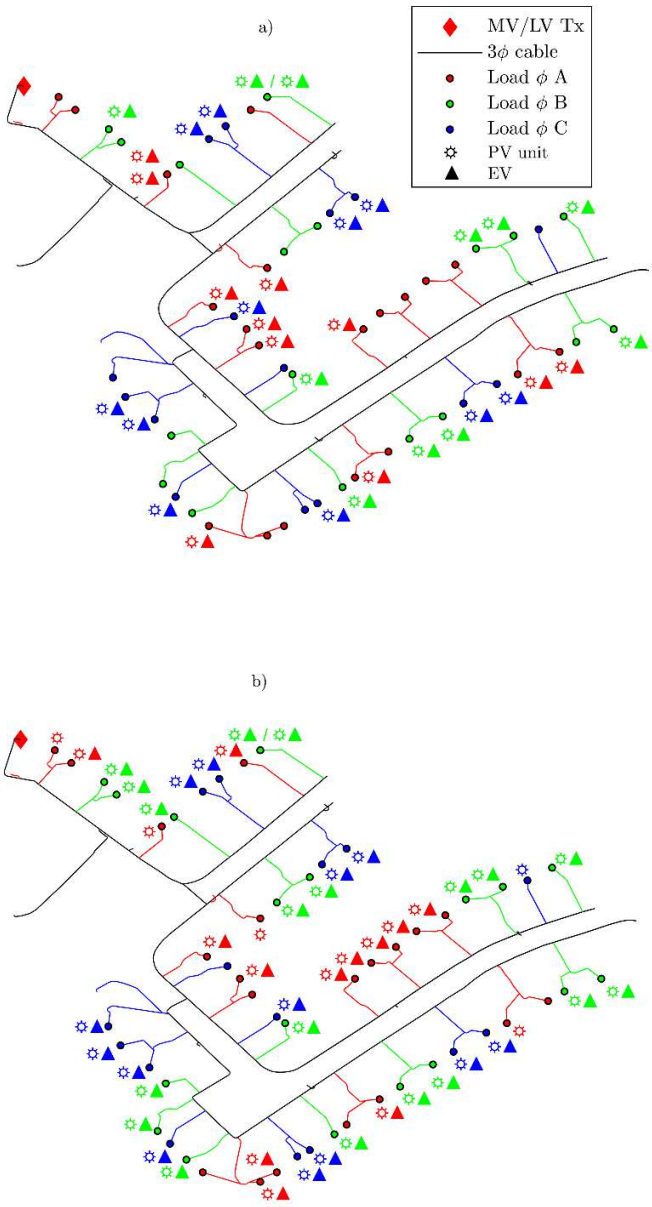


Fig. 6. Low-voltage test feeder for a) 60% of PV and EVs, b) 90% for PVs and 80% for EVs

Initially, a penetration level of 60% for both the EVs and PVs in the feeder was considered. This means that 33 of the 55 households have both a PV and EV operating at certain time slots of the test period. This penetration level was deemed appropriate to assess the robustness of the proposed control charging strategy. However, in a scenario with a higher penetration level of EVs and PVs, without a proper control action, the required charging power would increase significantly in hours of high demand, decreasing the correlation with the PV output power. Therefore, this may cause an undesired operating condition in the LV network. Thereby, to demonstrate the need to use network restrictions under these conditions, a case with a penetration level of 90% of PV units and 80% of EVs for the winter case was evaluated. In this scenario, the method described in Sections 2 and 3 was employed with and without network constraints (*i.e.*, Eqs. (19)–(21)). Both the EVs and PVs were randomly assigned among the households using a discrete uniform distribution $U\{1, 55\}$. The number of EVs and PVs connected per phase are presented in Table 2. The location of each EV and PV for both cases is shown in Fig. 6 and detailed in Appendix C.

Households with EVs are equipped with a single-phase charging spot of 3.7 *kW* via a standard AC connection. The charger efficiency is assumed to be $\eta_{ch} = 0.92$ [17]. The fixed variation for the rate of charge $(\Delta_P)$ in constraint (15) is set at 0.5 *kW*. In the first case, all EVs are simulated based on the specifications for a Nissan Leaf [29]: $BC = 24$ *kWh* and $ECR = 0.1778$ *kWh/km*. For simulating an EV with a higher energy requirement, in the second case, the electric Kia Soul (2018) [30] ($BC = 30$ *kWh* and $ECR = 0.1679$ *kWh/km*) was considered. For both cases, the battery energy levels are constrained to a $SOC_{\min} = 0.2$ and $SOC_{\max} = 0.95$ to avoid permanent battery damage or early ageing. Although the desired state-of-charge $SOC_{obj}$ depends on the user's driving needs, for simulation purpose, this was set to reach the $SOC_{\max}$.

Regarding the model presented in Section 3 and considering that residential PV systems can vary in a range from 2 to 5 *kW* [31], the PV units size at the evaluated households was limited to $P_i = 3.7$ kW, which is the maximum power for summer, with a unity power factor. However, for the winter season, a maximum power $P_i = 0.8$ *kW* was defined, as shown in Fig. 3. Additionally, the maximum and minimum allowable voltage at each time step is set to 0.9 *p.u.* and 1.1 *p.u.* The rated capacity of the main cable is 215 *A* (*i.e.*, $P_{Line\,1}^{\max} = 47.17$ *kW* per phase, assuming a lagging power factor of 0.95).

By considering that the initial penetration level is the most likely occurrence condition in the near future, one hundred series of simulations were carried out using the LV feeder in Fig. 6 a) for both the winter and summer seasons to prove the effectiveness of the proposed method. The first simulation was executed following the flowchart in Fig. 5, and the remaining ones were performed starting from step 3 to 6. As the second case is a critical situation with less probability of occurrence, only a single simulation was carried out to assess the need for the proposed network constraints. Simulations were run for a test period $T = 30$ hours (*i.e.*, starting from 00:00 to 06:00 the next day) with a 10-minute interval (*i.e.*, 180 slots of time). The proposed model in Eqs. (13)–(21) is solved by CPLEX 12.9 under its API in Python (DOcplex).

Table 2.
Number of EVs and PVs connected per phase and penetration level

| | Case | 1 | | 2 | |
|---|---|---|---|---|---|
| | Number of Households | EVs | PVs | EVs | PVs |
| Phase A | 21 | 11 | 11 | 12 | 16 |
| Phase B | 19 | 11 | 11 | 19 | 19 |
| Phase C | 15 | 11 | 11 | 13 | 14 |
| Total | 55 | 33 | 33 | 44 | 49 |

## 5. Results

By using the uncertainty criteria for the EVs presented in Section 2.1, the arrival time of EVs at home is randomly selected with a mean at 16:00 hours and a standard deviation of 3-h for both winter and summer. This was computed for the 100 simulations run per season, as shown in the boxplot of Fig. 7 a) and b). In both figures, the mean value of EVs that arrive at home per hour for winter and summer is represented by the green and magenta lines, respectively. For those EVs that arrive late, it is expected that these would charge up to the early morning.

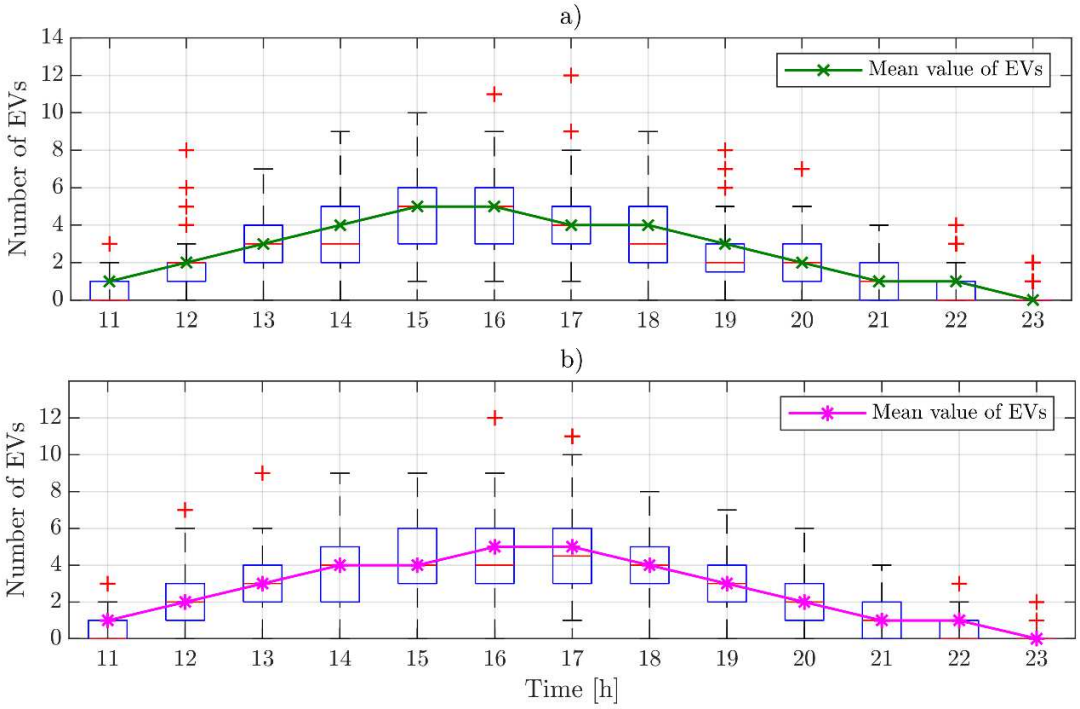


Fig. 7. Boxplot and mean value of EV arrival time during a) winter and b) summer in case 1

Under the premise that the aggregator can manage the embedded control unit of each EV charger and monitoring the PV inverters from a remote location, Fig. 8–10 show how such control actions limit the loading level on the main service cable when connecting the EVs and PVs for winter and summer, respectively. Due to the lower number of solar radiation hours during winter, PV generation is much lower compared to the summer case, and hence, the reverse power flow on the main cable. In Fig. 8 and 9, although phase A displays an initial higher loading level from 16:00 hours to 21:00 hours, the average

loading level in all phases for that time range is always below the rated capacity of the main cable. Even with some charging outliers, the proposed control strategy limits the loading level on the main cable to its nominal value while ensuring the desired charging level of all EVs. The outliers from midnight to the early morning occur because some EVs arrive with a low energy level or come late for charging.

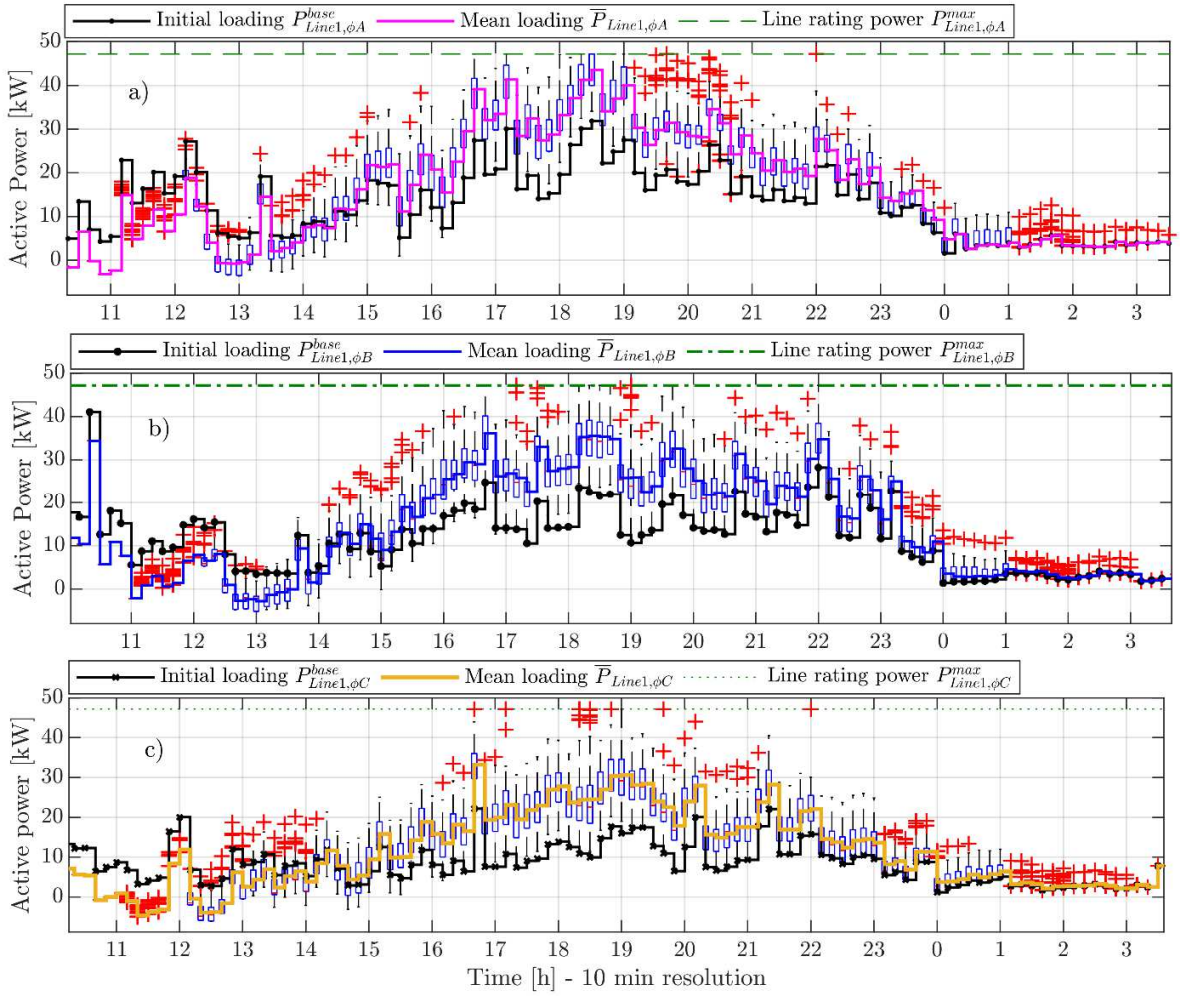


Fig. 8. Boxplot of loading level per phase on the feeder's main cable based on 100 optimisation scenarios for winter in case 1

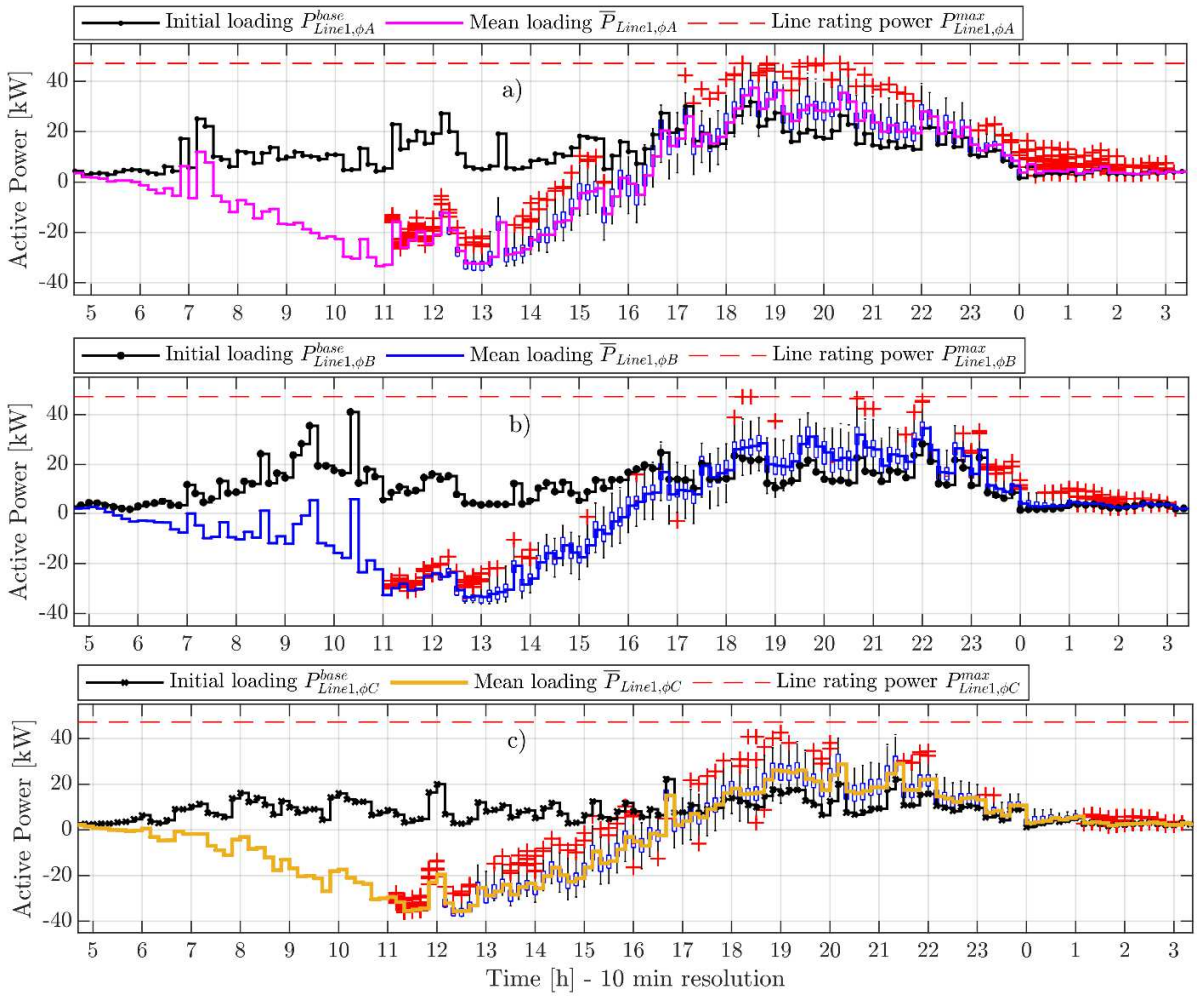


Fig. 9. Boxplot of loading level per phase on the feeder's main cable based on 100 optimisation scenarios for summer in case 1

On the other hand, the three-phase average loading level is below 83 *kW* from 16:30 hours to 20:00 hours during summer compared to winter thanks to the remaining PV energy downstream, which is used by the household loads and the EVs, as shown in Fig. 10. Since no control actions over PV generation are considered, it is assumed that the surplus power is injected into the network by selling it to the DSO.

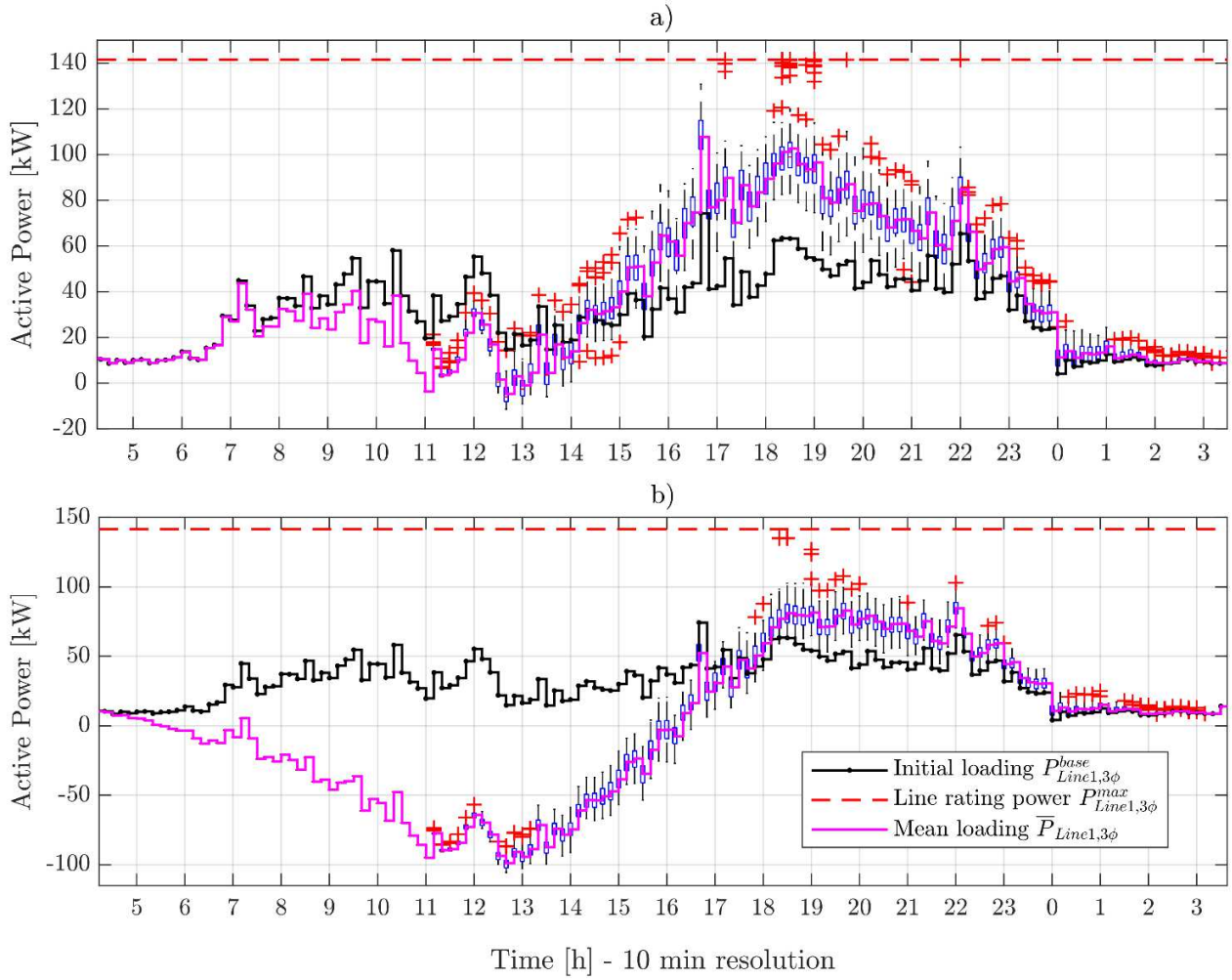


Fig. 10. Boxplot of loading level for the three-phase main cable based on 100 optimisation scenarios for a) winter and b) summer in case 1

For comparison, Fig. 11 shows the aggregated charging power for the winter scenario if an uncontrolled charging event would occur, along with the aggregated charging profiles using the proposed control method with and without network constraints. As the PV generation is low during the winter, the self-consumption for charging the EVs tends to be reduced, which increases the loading level of the main cable, as seen in Fig. 12. In this figure, the improvement of the loading level per phase on the main cable is achieved by considering network constraints.

On the other hand, if only constraints for power- and energy-boundaries are considered, this can produce overload events at any phase during the simultaneous charging process, as shown in Fig. 12. Therefore, if the optimisation problem does not consider the proposed network constraints, a safe operative condition for the LV network cannot be guaranteed.

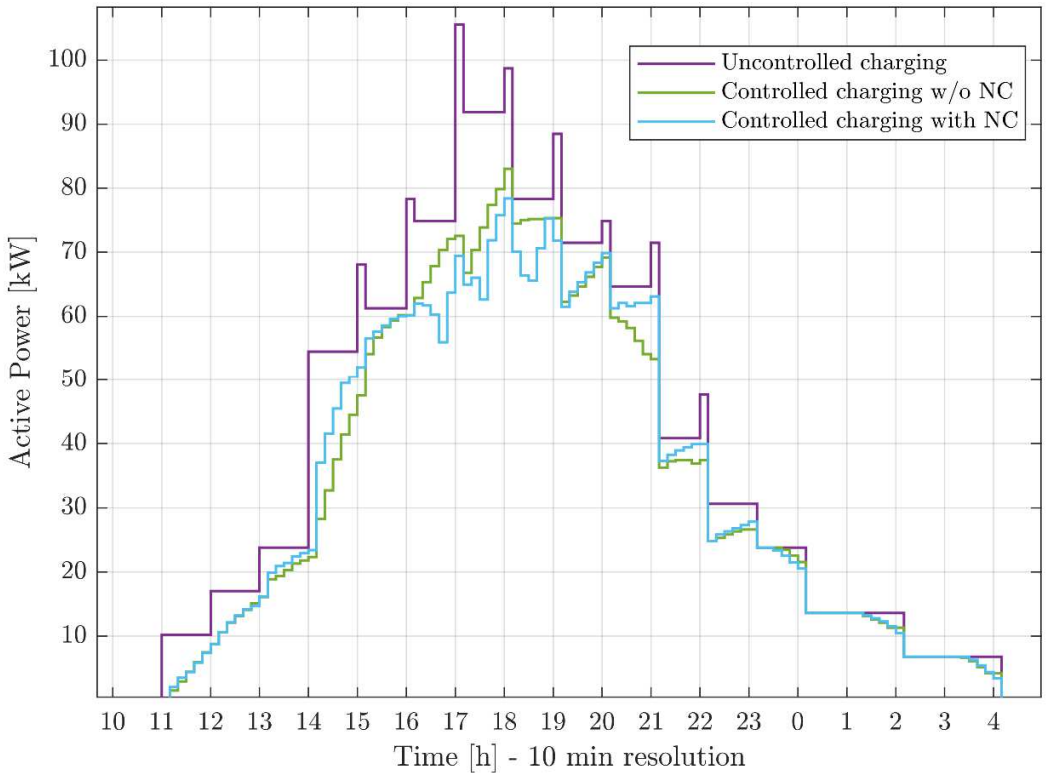


Fig. 11. Comparison between uncontrolled- and controlled charging with and without network constraints (NC) in case 2

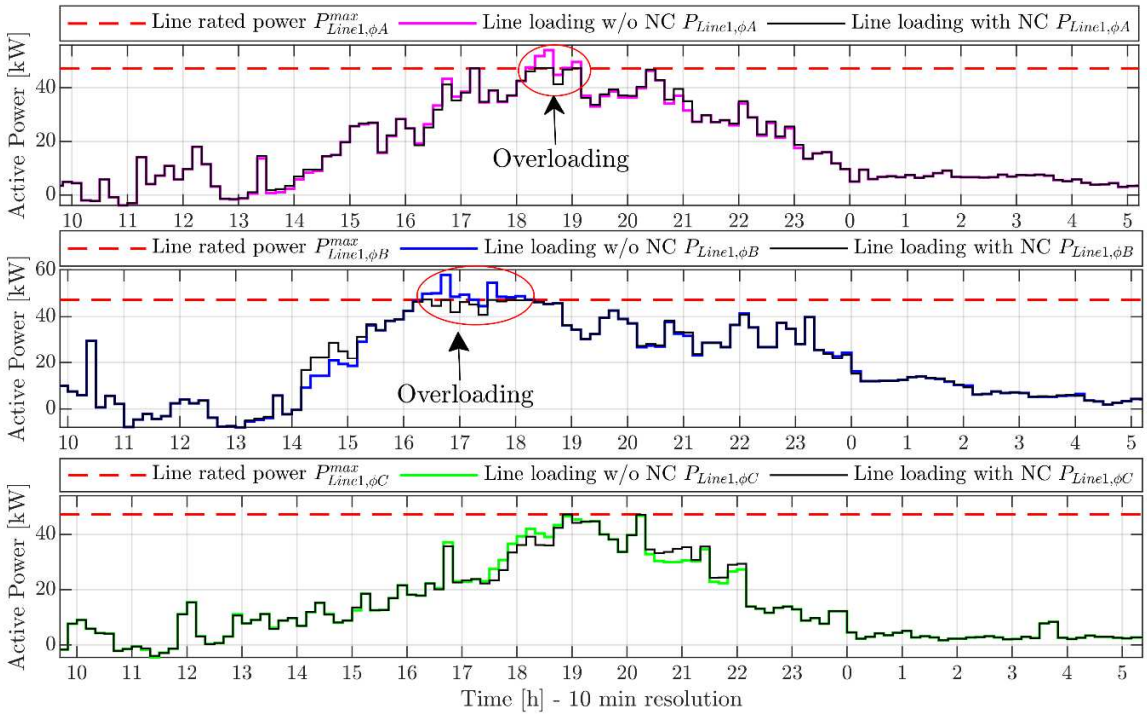


Fig. 12. Comparison of the loading level per phase with and without network constraints (NC) in case 2

Due to the rated power of the distribution transformer is much higher than that of the main cable, for this particular feeder, constraint (21) would not be violated. Therefore, by applying the optimisation method, the power level on the LV side of the distribution transformer will be equal to the one on the service cable.

As an example to demonstrate that the proposed approximation (Eq. (19)) is valid, two scenarios from case 1 were analysed, *i.e.*, scenarios 97 (winter) and 51 (summer). Fig. 13 and 14 show how voltage at household 53, which is located at the end of the feeder, is affected by the charging process and generation from other EVs and PVs. Both figures compare the initial voltage profile, the one computed from the optimisation and the one obtained using the quasi-dynamic load flow in *PF*. The second relies on utilising the sensitivity coefficients (*SC*), the optimised charging profiles of EVs and the expected PV power. The latter voltage profile is resulting from uploading the optimised charging profiles of EVs in *PF*. For both scenarios, all voltage values are within the operational limits of the network, which indicates that the voltage level is not the binding constraint for this particular feeder, and therefore the focus for the results will be on the loading levels, as shown in Fig. 8–10 and 12.

Accuracy of the optimisation method was proved through the error in voltage computation from the results for both cases, as shown in Fig. 15 and 16. Voltage error along the test period was less than 0.2% and 2% for winter and summer, respectively. These values differ from one season to another due to there is a higher level of PV generation which increases the losses on the feeder, and only one set of *SC* along the test period is used. Now, if we compare the previous winter scenario with the second case (Fig. 15a) and 16), it is observed that the addition of new EVs and PVs will increase the voltage error due to just one set of sensitivity coefficients is following all changes in load during the test period. However, the error is still less than 1%, and hence, this exemplifies that the proposed linearization is still valid for a massive penetration level.

Note that depending on the irradiance level, temperature and the load demand, the reverse power flow and its impact on voltage rise due to PV power will be at the most severe state at noon. This is when PV output power is at its maximum level, and power demand is the lowest. However, this condition can be mitigated by charging the EVs, taking advantage of the correlation that exists between them and the PVs. Therefore, thanks to the sensitivity coefficients for PV units in both loading and voltage level within the network restrictions, it is possible to reproduce such operative condition, as seen in Fig. 8–10 and Fig. 12–14.

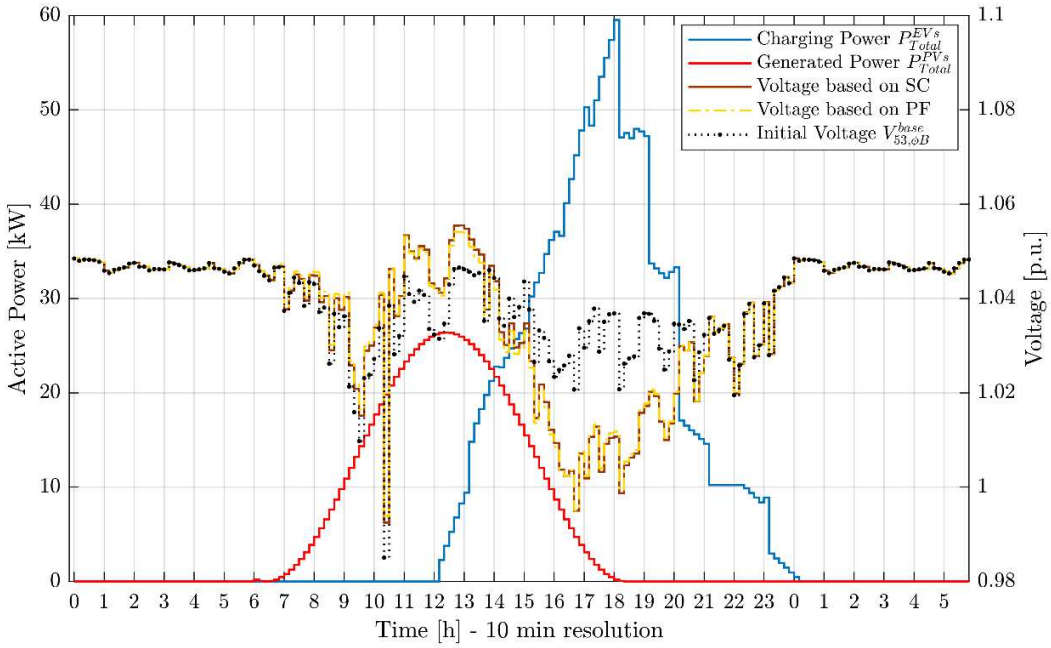


Fig. 13. Voltage profile at Load 53 due to the effect of total charging power and the PV power during winter (case 1, scenario 97)

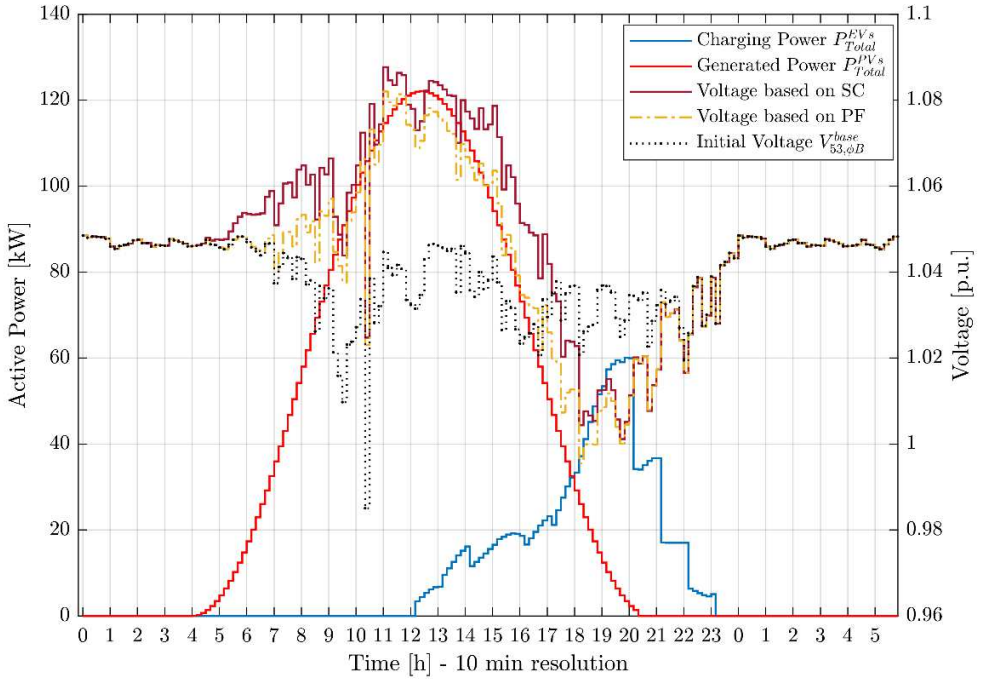


Fig. 14. Voltage profile at household 53 due to the effect of total charging power and the PV power during summer (case 1, scenario 51)

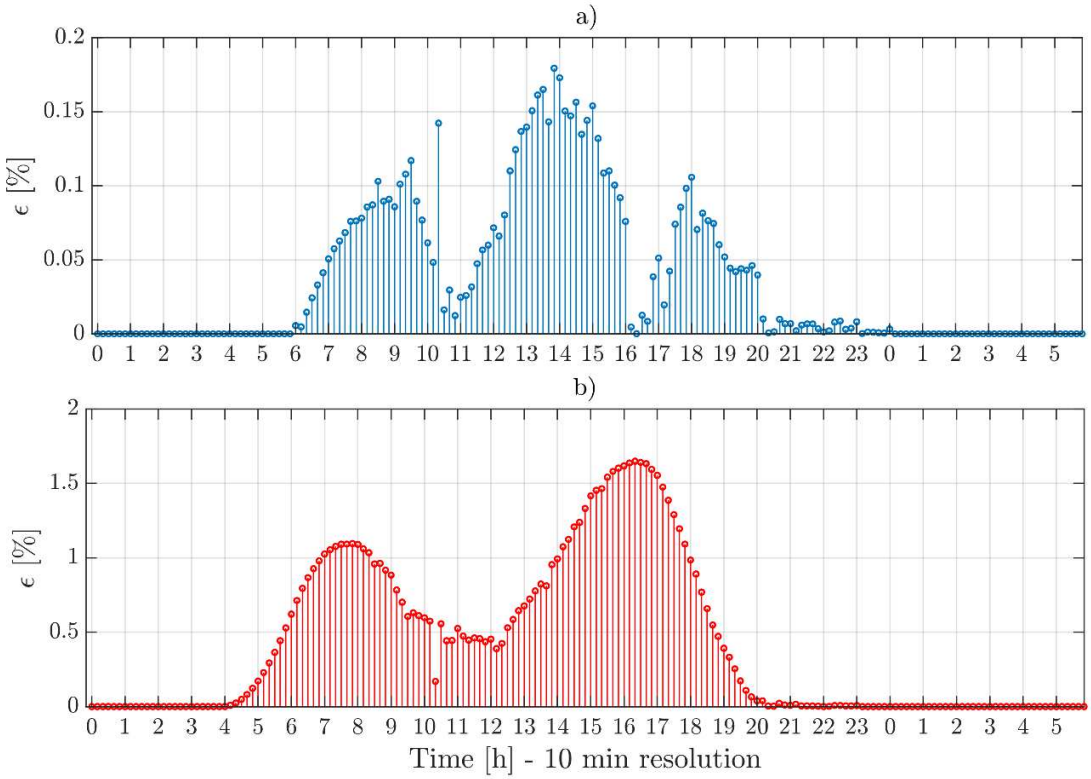


Fig. 15. Voltage error at Load 53 by using the sensitivity coefficients for a) winter and b) summer in case 1

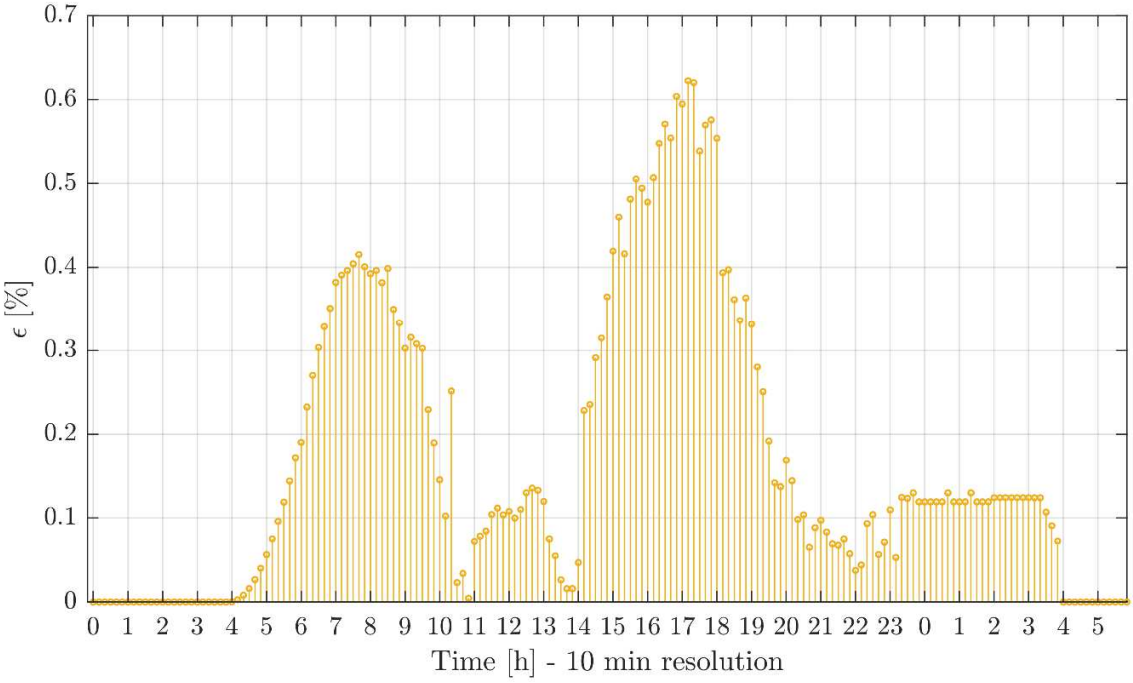


Fig. 16. Voltage error at Load 53 by using the sensitivity coefficients in a higher penetration level of PVs and EVs in winter (case 2)

5.1. Electric vehicles energy requirement

In order to show the effectiveness of the proposed centralised charging strategy, it has been extracted four cases of EVs with different charging patterns and energy trajectories from scenario 51 (*i.e.*, the case with a penetration level of 60%), as given in Fig. 17 and 18, respectively. These results come out of the parameters defined in Section 4 and a daily travelled distance $d_j = \{34, 78, 61, 41\}$ in *km* for EVs located at households 4, 20, 45 and 54, respectively.

Fig. 17 shows the optimal charging pattern, time availability and power generated for the selected EVs and PVs. It is observed that the charging profiles satisfy both the objective function and constraints (14)–(16). For comparison, in Fig. 17a), the pre-set value of $\Delta_P$ is kept during the charging process, whereas in Fig. 17d), *e.g.*, the penalty deviation variable was used at time interval 92 to reach the required energy level faster due to its shorter time window in comparison to the one in other EVs. It is also noted that the proposed charging strategy automatically delays the charging process, when it is necessary, to meet the charging demand of all EVs. Besides, it can be seen that the EVs with an early arrival take advantage of PV output power to be charged. This significantly reduces the load level on the main service cable.

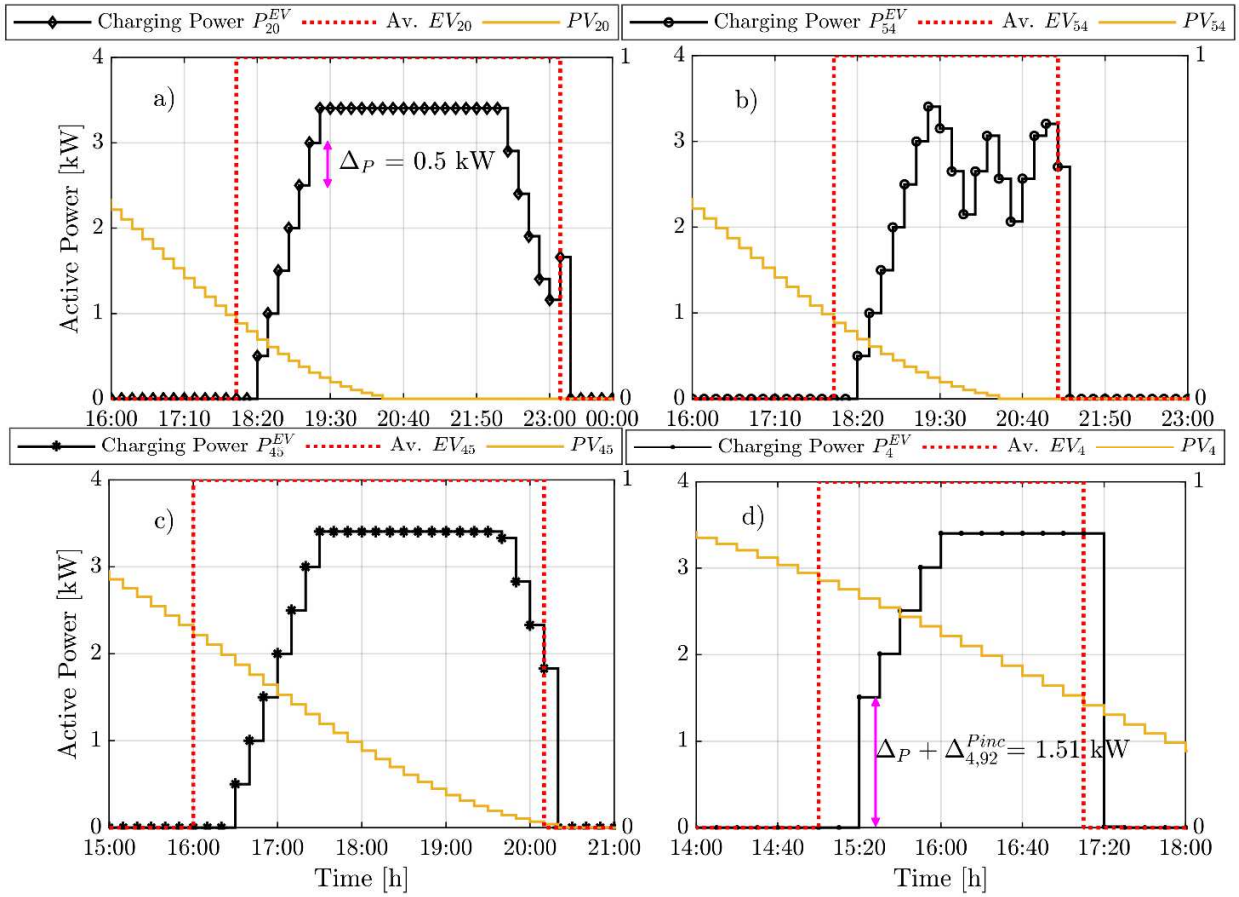


Fig. 17. Optimal charging profiles for the EVs located at households a) 20, b) 54, c) 45 and d) 4 in case 1

Fig. 18 reflects the energy paths from the selected EVs, which were obtained using the proposed control strategy. These energy trajectories correspond to the charging profiles in Fig. 17. To exemplify the energy requirements of EVs, in Fig. 18a), for the EV at household 20 the arrival energy is $e_{20}^{arr} = (24 \times 0.95) - (0.1778 \times 78) = 8.93\,kWh$ while the objective energy level is $e_{20}^{req} = \left((24 \times 0.95) - 8.93\right)/0.92 = 15.07\,kWh$ for a parking time of $t_{20}^{p} = ceil\{15.07/3.7\} = 5\text{-h}$, which is equivalent to $t_{20}^{\text{int}} = 5/(10/60) = 30$ intervals of 10 minutes. These calculations were carried out in all simulations according to step three from Fig. 5.

When the energy boundaries are too narrow, or the charging process is delayed, the energy trajectory tends to move towards the lower energy boundary, as shown in Fig. 18c) and d). However, for EVs with a longer charging time and a slight delay, the energy path would go through the middle of the energy boundaries, as given in Fig. 18a). On the other hand, if charging power varies once its rated capacity has been reached (Fig. 17b)), the energy trajectory would vary accordingly to these changes until meeting the required energy state, as depicted in Fig. 18b). Therefore, these results confirm the effectiveness of the proposed method.

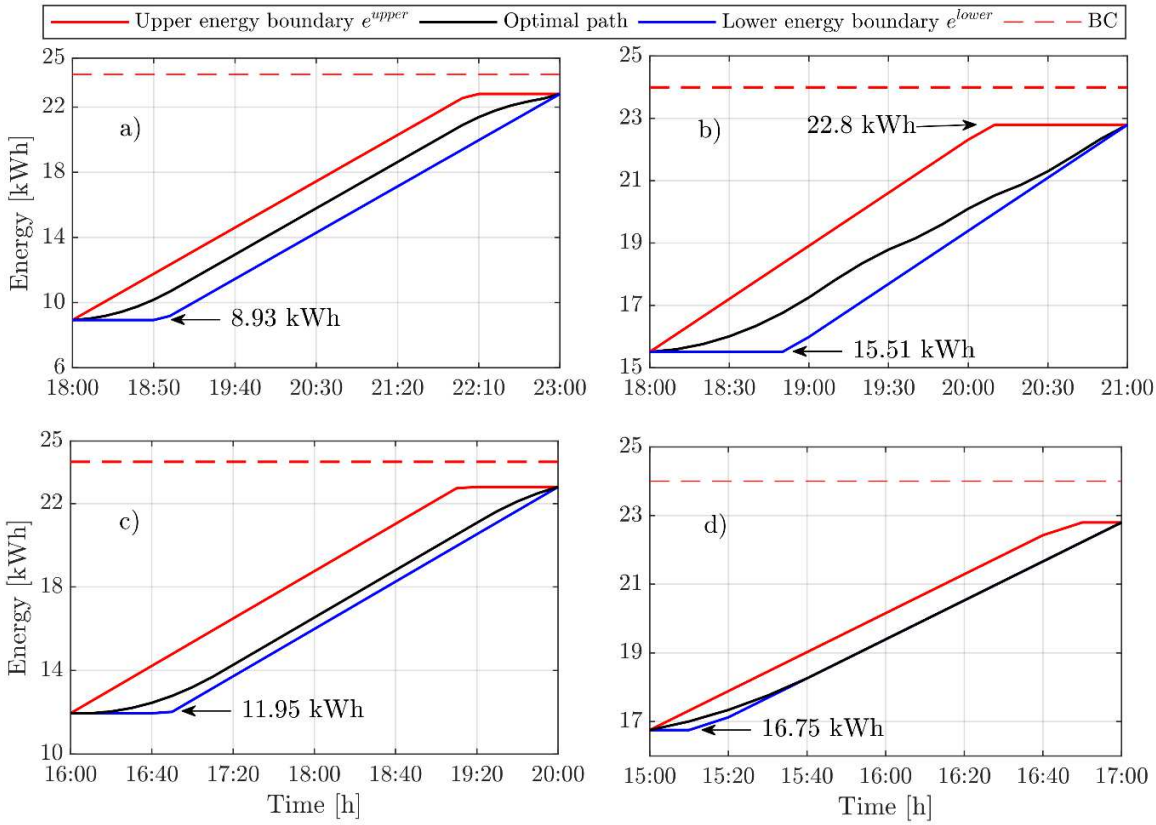


Fig. 18. Optimal energy trajectories for the EVs located at households a) 20, b) 54, c) 45 and d) 4 in case 1

## 6. Conclusions

This article has developed a new charging strategy to find in a decentralised fashion the best charging pattern that meets the energy requirements of each EVs connected to the LV network while taking advantage of the PV generation and maintaining the network within its operational limits. Another contribution is the development of an energy boundary model for EVs, which ensures that the proposed charging strategy finds an optimal charging path by dynamically adjusting a variable charging rate in conjunction with a fixed one to assure the technical limits of the network. This model is based on the daily travelled distance, arrival time, battery capacity and energy consumption rate. Moreover, a mathematical approximation for modelling the uncertainty of PV output power was also proposed, which was based on the appraisement of real data of irradiance and ambient temperature. The proposed strategy exploits the use of network sensitivity coefficients by linearizing both the loading levels and voltages of the network. This methodology is verified using real data from an LV feeder and load demand for winter and summer. Numerical results demonstrate that the proposed charging strategy is feasible and effective for finding the optimal charging profile of each EV while addressing network constraints. Besides, this charging strategy ensures an even distribution of charging power at each time slot for all EVs. Further, the proposed method can also be extended to define the most suitable PV export limits if exist a tighter requirement concerning the voltage level or loading level on the assets of the DSO.

**Acknowledgements**

This work was supported by TECNALIA funding through its PhD scholarship program. The authors also would like to thank the Basque Government (GISEL research group IT1191-19) and the UPV/EHU (GISEL research group 18/181) for their support in this work.

**Data Availability**

Supplementary data related to this research can be found at

**Appendix A. Probability density functions for EV's behaviour**

Lognormal probability distribution

If the logarithm of $X$ is normally distributed $\ln(x) \sim N(\mu, \sigma^2)$, the lognormal probability distribution function with parameters $\mu$ and σ of the logarithmic values can be expressed as the Eq. (23).

$$f(x \mid \mu, \sigma) = \frac{\exp\left\{-(\ln(x)-\mu)^2 \Big/ (2\cdot\sigma^2)\right\}}{x\cdot\sigma\cdot\sqrt{2\cdot\pi}} \tag{23}$$

Truncate probability distribution

If $X$ is a continuous random variable normally distributed $N(\mu, \sigma^2)$ with mean $\mu$ and standard deviation $\sigma$, and an expected value within the range $(a, b)$. The truncated normal probability density function $\varphi$ is given by Eq. (24).

$$\varphi(x \mid \mu, \sigma, a, b) = \frac{\frac{1}{\sigma} \cdot \Phi\left(\frac{x-\mu}{\sigma}\right)}{\Phi\left(\frac{b-\mu}{\sigma}\right) - \Phi\left(\frac{a-\mu}{\sigma}\right)} \tag{24}$$

## Appendix B. PV system model parameters

Several major design parameters for the PV model are presented in Tables B.1 and B.2 as a reference.

Table B.1
Parameters of the PV module and inverter for the Araujo-Green model

| Parameter | Value | Unit |
|---|---|---|
| $I_{scn}$ | 8.83 | *A* |
| $V_{ocn}$ | 37.4 | *V* |
| $I_{mpp}$ | 8.31 | *A* |
| $V_{mpp}$ | 30.1 | *V* |
| *NOCT* | 45 | *ºC* |
| $N_p$ | 1 | |
| $N_s$ | 15 | |
| *k* | $1.3806503 \cdot 10^{-23}$ | *J/K* |
| *q* | $1.60217646 \cdot 10^{-19}$ | *C* |
| $G_{STC}$ | 1000 | $W/m^2$ |
| $T_{ref}$ | 25 | *ºC* |
| $\beta$ | 0.0023 | $ºC^{-1}$ |
| $\eta_{inv}$ | 0.99 | |

Table B.2
Parameters for the approximation of the PV inverter output power

| Parameter | Summer | Winter |
|---|---|---|
| *a* | 5/7 | 1 |
| *b* | 2 | 2 |
| *c* | 6 | 4 |
| *d* | *3* | 2 |

## Appendix C.

In Table C.1., rows highlighted in blue represent the EVs and PVs connected to a particular household whose results were displayed in Fig. 17 and 18. The red rows in Tables C.2. and Table C.3. depicts the household chosen to exemplify the impact of charging and generation in voltage profile, as shown in Fig. 13–16. These users were selected by taking into account their location and phase on the feeder in order to show the performance of the proposed decentralised charging strategy on the network.

Table C.4.
Location of EVs and PVs in the test feeder for a penetration level of 60%

| EV & PV | Load | Node | Phase | EV & PV | Load | Node | Phase |
|---|---|---|---|---|---|---|---|
| 1 | 47 | 835 | C | 18 | 46 | 817 | A |
| 2 | 39 | 701 | C | 19 | 10 | 248 | B |
| 3 | 2 | 47 | B | 20 | 41 | 755 | B |
| 4 | 55 | 906 | A | 21 | 43 | 780 | C |
| 5 | 14 | 289 | A | 22 | 4 | 73 | A |
| 6 | 19 | 342 | C | 23 | 45 | 813 | B |

| | | | | | | | |
|---|---|---|---|---|---|---|---|
| 7 | 27 | 539 | C | 24 | 22 | 388 | A |
| 8 | 28 | 556 | C | 25 | 12 | 264 | C |
| 9 | 52 | 898 | A | 26 | 53 | 899 | B |
| 10 | 32 | 614 | C | 27 | 8 | 208 | C |
| 11 | 40 | 702 | B | 28 | 36 | 676 | B |
| 12 | 54 | 900 | A | 29 | 34 | 629 | A |
| 13 | 5 | 74 | A | 30 | 17 | 327 | C |
| 14 | 35 | 639 | B | 31 | 11 | 249 | B |
| 15 | 21 | 387 | A | 32 | 16 | 320 | C |
| 16 | 23 | 406 | B | 33 | 37 | 682 | B |
| 17 | 20 | 349 | A | | | | |

Table C.5.
Location of EVs and PVs in the test feeder for a penetration level of 80% for EVs and 90% for PVs

| Load | Node | Phase | PV | EV | Load | Node | Phase | PV | EV |
|---|---|---|---|---|---|---|---|---|---|
| 01 | 34 | A | 1 | 1 | 29 | 562 | A | 26 | 26 |
| 02 | 47 | B | 2 | 2 | 30 | 563 | A | 27 | 27 |
| 03 | 70 | A | 3 | - | 31 | 611 | A | 28 | 28 |
| 04 | 73 | A | 4 | - | 32 | 614 | C | 29 | 29 |
| 06 | 83 | B | 5 | 5 | 33 | 619 | C | 30 | - |
| 07 | 178 | B | 6 | 6 | 34 | 629 | A | 31 | 31 |
| 08 | 208 | C | 7 | 7 | 35 | 639 | B | 32 | 32 |
| 09 | 225 | A | 8 | 8 | 36 | 676 | B | 33 | 33 |
| 10 | 248 | B | 9 | 9 | 37 | 682 | B | 34 | 34 |
| 11 | 249 | B | 10 | 10 | 38 | 688 | B | 35 | 35 |
| 12 | 264 | C | 11 | 11 | 39 | 701 | C | 36 | 36 |
| 13 | 276 | B | 12 | 12 | 40 | 702 | B | 37 | 37 |
| 14 | 289 | A | 13 | - | 41 | 755 | B | 38 | 38 |
| 15 | 314 | B | 14 | 14 | 42 | 778 | C | 39 | 39 |
| 16 | 320 | C | 15 | 15 | 43 | 780 | C | 40 | 40 |
| 17 | 327 | C | 16 | 16 | 44 | 785 | B | 41 | 41 |
| 18 | 337 | C | 17 | 17 | 45 | 813 | B | 42 | 42 |
| 21 | 387 | A | 18 | 18 | 47 | 835 | C | 43 | 43 |
| 22 | 388 | A | 19 | 19 | 48 | 860 | A | 44 | 44 |
| 23 | 406 | B | 20 | 20 | 49 | 861 | A | 45 | 45 |
| 24 | 458 | C | 21 | 21 | 50 | 886 | B | 46 | 46 |
| 25 | 502 | A | 22 | 22 | 51 | 896 | A | 47 | 47 |
| 26 | 522 | B | 23 | 23 | 52 | 898 | A | 48 | - |
| 27 | 539 | C | 24 | 24 | 53 | 899 | B | 49 | 49 |
| 28 | 556 | C | 25 | 25 | | | | | |

## References


[1] P. Richardson, D. Flynn, A. Keane, Local versus centralized charging strategies for electric vehicles in low voltage distribution systems, IEEE Transactions on Smart Grid. 3 (2012) 1020–1028. https://doi.org/10.1109/TSG.2012.2185523.

[2] J. García-Villalobos, I. Zamora, J.I. San Martín, F.J. Asensio, V. Aperribay, Plug-in electric vehicles in electric distribution networks: A review of smart charging approaches, Renewable and Sustainable Energy Reviews. 38 (2014) 717–731. https://doi.org/10.1016/j.rser.2014.07.040.

[3] F. Mwasilu, J.J. Justo, E.K. Kim, T.D. Do, J.W. Jung, Electric vehicles and smart grid interaction: A review on vehicle to grid and renewable energy sources integration, Renewable and Sustainable Energy Reviews. 34 (2014) 501–516. https://doi.org/10.1016/j.rser.2014.03.031.

[4] S. Hajforoosh, M.A.S. Masoum, S.M. Islam, Online optimal variable charge-rate coordination of plug-in electric vehicles to maximize customer satisfaction and improve grid performance, Electric Power Systems Research. 141 (2016) 407–420.

https://doi.org/10.1016/j.epsr.2016.08.017.

[5] M.J.E. Alam, K.M. Muttaqi, D. Sutanto, Effective Utilization of Available PEV Battery Capacity for Mitigation of Solar PV Impact and Grid Support with Integrated V2G Functionality, IEEE Transactions on Smart Grid. 7 (2016) 1562–1571. https://doi.org/10.1109/TSG.2015.2487514.

[6] Q. Hoarau, Y. Perez, Interactions between electric mobility and photovoltaic generation: A review, Renewable and Sustainable Energy Reviews. 94 (2018) 510–522. https://doi.org/10.1016/j.rser.2018.06.039.

[7] K.E. Antoniadou-Plytaria, I.N. Kouveliotis-Lysikatos, P.S. Georgilakis, N.D. Hatziargyriou, Distributed and Decentralized Voltage Control of Smart Distribution Networks: Models, Methods, and Future Research, IEEE Transactions on Smart Grid. 8 (2017) 2999–3008. https://doi.org/10.1109/TSG.2017.2679238.

[8] T.R.F. Mendonca, T.C. Green, Distributed Active Network Management Based on Locally Estimated Voltage Sensitivity, IEEE Access. 7 (2019) 105173–105185. https://doi.org/10.1109/ACCESS.2019.2931955.

[9] P. Richardson, D. Flynn, A. Keane, Optimal charging of electric vehicles in low-voltage distribution systems, IEEE Transactions on Power Systems. 27 (2012) 268–279. https://doi.org/10.1109/TPWRS.2011.2158247.

[10] A. O'Connell, D. Flynn, A. Keane, Rolling multi-period optimization to control electric vehicle charging in distribution networks, IEEE Transactions on Power Systems. 29 (2014) 340–348. https://doi.org/10.1109/TPWRS.2013.2279276.

[11] M. Esmaili, A. Goldoust, Multi-objective optimal charging of plug-in electric vehicles in unbalanced distribution networks, International Journal of Electrical Power & Energy Systems. 73 (2015) 644–652. https://doi.org/10.1016/j.ijepes.2015.06.001.

[12] H.F. Farahani, Improving voltage unbalance of low-voltage distribution networks using plug-in electric vehicles, Journal of Cleaner Production. 148 (2017) 336–346. https://doi.org/10.1016/j.jclepro.2017.01.178.

[13] F. Marra, G.Y. Yang, C. Traeholt, E. Larsen, J. Ostergaard, B. Blazic, W. Deprez, EV charging facilities and their application in LV feeders with photovoltaics, IEEE Transactions on Smart Grid. 4 (2013) 1533–1540. https://doi.org/10.1109/TSG.2013.2271489.

[14] H. Zhang, Z. Hu, Z. Xu, Y. Song, Evaluation of Achievable Vehicle-to-Grid Capacity Using Aggregate PEV Model, IEEE Transactions on Power Systems. 32 (2017) 784–794. https://doi.org/10.1109/TPWRS.2016.2561296.

[15] Q. Chen, N. Liu, C. Hu, L. Wang, J. Zhang, Autonomous Energy Management Strategy for Solid-State Transformer to Integrate PV-Assisted EV Charging Station Participating in Ancillary Service, IEEE Transactions on Industrial Informatics. 13 (2017) 258–269. https://doi.org/10.1109/TII.2016.2626302.

[16] O. Sundstrom, C. Binding, Flexible Charging Optimization for Electric Vehicles Considering Distribution Grid Constraints, IEEE Transactions on Smart Grid. 3 (2012) 26–37. https://doi.org/10.1109/TSG.2011.2168431.

[17] Z. Xu, Z. Hu, Y. Song, W. Zhao, Y. Zhang, Coordination of PEVs charging across multiple aggregators, Applied Energy. 136 (2014) 582–589. https://doi.org/10.1016/j.apenergy.2014.08.116.

[18] Z. Xu, W. Su, Z. Hu, Y. Song, H. Zhang, A Hierarchical Framework for Coordinated Charging of Plug-In Electric Vehicles in China, IEEE Transactions on Smart Grid. 7 (2016) 428–438. https://doi.org/10.1109/TSG.2014.2387436.

[19] National Renewable Energy Laboratory, Transportation Secure Data Center, (2017). www.nrel.gov/tsdc.

[20] M. Shafie-Khah, E. Heydarian-Forushani, G.J. Osorio, F.A.S. Gil, J. Aghaei, M. Barani, J.P.S. Catalao, Optimal Behavior of Electric Vehicle Parking Lots as Demand Response Aggregation Agents, IEEE Transactions on Smart Grid. 7 (2016) 2654–2665. https://doi.org/10.1109/TSG.2015.2496796.

[21] A. Cortés, J. Merino, E. Torres, Stochastic Generation of Aggregated Charging Profiles of PEVs for the Operation Analysis of Low Voltage Networks, in: CIRED, Madrid, 2019: pp. 1–5. https://cired-repository.org/handle/20.500.12455/448.

[22] J. Van Roy, N. Leemput, F. Geth, R. Salenbien, J. Buscher, J. Driesen, Apartment Building Electricity System Impact of Operational Electric Vehicle Charging Strategies, IEEE Transactions on Sustainable Energy. 5 (2014) 264–272. https://doi.org/10.1109/TSTE.2013.2281463.

[23] Weather stations: readings collected in 2017, Open Data Euskadi. (2018). https://opendata.euskadi.eus/catalogo/-/estaciones-meteorologicas-lecturas-recogidas-en-2017/ (accessed January 8, 2018).

[24] C. Rus-casas, J.D. Aguilar, P. Rodrigo, F. Almonacid, P.J. Pérez-higueras, Classification of methods for annual energy harvesting calculations of photovoltaic generators, Energy Conversion and Management. 78 (2014) 527–536. https://doi.org/10.1016/j.enconman.2013.11.006.

[25] ‘DIgSILENT GmbH Germany, DIgSILENT PowerFactory, (2019). https://www.digsilent.de/en/.

[26] Python 3.6.6, (2018). https://www.python.org/downloads/release/python-366/ (accessed June 27, 2018).

[27] A.N. Espinosa, L. (Nando) Ochoa, Dissemination Document “ Low Voltage Networks Models and Low Carbon Technology Profiles ,” 2015. https://doi.org/10.13140/RG.2.1.2216.1366.

[28] Electriciy North West, Low Voltage Network Solutions, (2019). https://www.enwl.co.uk/lvns (accessed August 20, 2018).

[29] U.S. Department of Energy, 2013 Nissan Leaf Advanced Vehicle Testing - Baseline Testing Results, 2015. http://www.transportation.anl.gov/D3/, (accessed June 20, 2018).

[30] 2018 Kia Soul EV Specifications, (2020). https://www.kiamedia.com/us/en/models/soul-ev/2018/specifications (accessed January 7, 2019).

[31] S.F. Santos, D.Z. Fitiwi, M. Shafie-khah, A.W. Bizuayehu, J.P.S. Catalão, Introduction to Renewable Energy Systems, in: Optimization in Renewable Energy Systems, Elsevier, 2017: pp. 1–26. https://doi.org/10.1016/B978-0-08-101041-9.00001-6.